LANDSLIDE AND LIQUEFACTION MAPS FOR THE OCEAN SHORES AND WESTPORT PENINSULAS, GRAYS HARBOR COUNTY, WASHINGTON: Effects on Tsunami Inundation Zones of a Cascadia Subduction Zone Earthquake

by Stephen L. Slaughter, Timothy J. Walsh,
Anton Ypma, and Recep Cakir

WASHINGTON
DIVISION OF GEOLOGY
AND EARTH RESOURCES
Report of Investigations 38
July 2014

WASHINGTON STATE DEPARTMENT OF
Natural Resources
Peter Goldmark - Commissioner of Public Lands

DISCLAIMER

Washington Department of Natural Resources
Division of Geology and Earth Resources

Mailing Address:
MS 47007
Olympia, WA 98504-7007

Street Address:
Natural Resources Bldg, Rm 148
1111 Washington St SE
Olympia, WA 98501

Phone: 360-902-1450; *Fax:* 360-902-1785
E-mail: geology@dnr.wa.gov
Website: http://www.dnr.wa.gov/geology

Publications List:
http://www.dnr.wa.gov/researchscience/topics/geologypublications library/pages/pubs.aspx

Online searchable catalog of the Washington Geology Library:
http://www.dnr.wa.gov/researchscience/topics/geologypublications library/pages/washbib.aspx

Washington State Geologic Information Portal:
http://www.dnr.wa.gov/geologyportal

Suggested Citation: Slaughter, S. L.; Walsh, T. J.; Ypma, Anton; Cakir, Recep, 2014, Landslide and liquefaction maps for the Ocean Shores and Westport peninsulas, Grays Harbor County, Washington: Effects on tsunami inundation zones of a Cascadia subduction zone earthquake: Washington Division of Geology and Earth Resources Report of Investigations 38, 3 sheets plus 26 p. text.

Published in the United States of America

Contents

FIGURES

TABLES

SHEETS

Landslide and Liquefaction Maps for the Ocean Shores and Westport Peninsulas, Grays Harbor County, Washington: Effects on Tsunami Inundation Zones of a Cascadia Subduction Zone Earthquake

Stephen L. Slaughter, Timothy J. Walsh, Anton Ypma, and Recep Cakir
Washington Division of Geology and Earth Resources
MS 47007; Olympia, WA 98504-7007

INTRODUCTION

The Washington Division of Geology and Earth Resources (WADGER) participates in the National Tsunami Hazard Mitigation Program to assess tsunami hazards along the Washington coast, particularly those generated by nearby faults such as the Cascadia subduction zone (CSZ). Currently, many coastal communities have tsunami evacuation routes and assembly areas based on mapping of potential inundation areas from a tsunami initiated by a CSZ earthquake on the Washington coast (WADGER, 2007a,b, 2012; Walsh and others, 2000, 2002a,b, 2003, 2005). These evacuation routes and evacuation areas had not been compared to areas of potential ground failure that could initiate from a CSZ earthquake. Earthquake-induced ground failures could adversely affect tsunami evacuation by blocking or damaging evacuation routes, potentially rendering them impassable, or impeding an efficient and rapid vehicular evacuation. We have concentrated part of our technical program on earthquake-induced ground failures, including soil liquefaction and landslides, in order to improve evacuation planning for tsunamis that would inundate coastal areas in less than an hour after earthquake ground shaking. This report assesses the earthquake-induced ground failure potential for the communities of Ocean Shores and Westport in Grays Harbor County, Washington (Fig. 1). Note that the peninsulas are officially named Point Brown to the north and Point Chehalis to the south; however, we will refer to the peninsulas as the respective cities built on them, Ocean Shores and Westport. We consider here both soil liquefaction and landslide initiation.

The probability of soil liquefaction increases with the duration of shaking (Seed and Idriss, 1982; Seed and others, 2003), and slopes that are stable under static conditions may fail under large ground accelerations (Keefer, 1984; Jibson and others, 1998). A CSZ event may produce a magnitude (M) 9+ earthquake (Satake and others, 2003) and would produce ground accelerations on the Washington coast of as much as 0.40 *g* (*g* is the acceleration due to gravity) and shaking durations of as much as several minutes (Art Frankel, U.S. Geological Survey, written commun., 2008), more than sufficient to initiate soil liquefaction and shallow landslides. Soil liquefaction can damage transportation networks, such as roads and bridges (Seed and others, 2003), and landslides, even very small landslides, can render a road impassable to automobiles. These ground failures can complicate or prohibit vehicular evacuation as well as hamper emergency response and recovery efforts.

The objective of this report is to assist city and emergency management officials in evaluating the suitability of existing evacuation routes and assembly areas for potential vulnerability to ground failure from a M9+ CSZ earthquake. Results of this report could necessitate modifying, adding, or removing current evacuation routes and assembly areas.

This report is not intended as a stand-alone geotechnical resource and does not involve an investigation into the performance of the built environment. However, understanding which areas are more vulnerable to ground failure during a large earthquake can help communities prepare for potentially obstructed transportation networks, toppled buildings, and other secondary seismic hazards. Likewise, we present no estimate of the damage resulting from liquefaction; in some instances, liquefaction may occur without causing significant ground displacement and consequent damages to structures.

The maps included in this report cannot be used to determine the presence or absence of liquefiable soils or landslide vulnerability in any specific locality. They are no substitute for a site-specific geotechnical investigation, which must be performed by qualified practitioners and is required to assess the potential for ground failures and consequent damage at a given locality.

SEISMICALLY INDUCED GROUND FAILURES

Soil Liquefaction

Liquefaction is a form of ground failure in which the strength and stiffness of a soil is reduced by earthquake shaking or other rapid loading. Liquefaction has been responsible for tremendous amounts of infrastructure damage in earthquakes around the world (Fig. 2), including western Washington. Liquefaction occurs in saturated soils that temporarily behave like a liquid as result of ground shaking (Grant and others, 1998). Prior to an earthquake, soil pore water pressure is relatively low; however, earthquake shaking can cause the water pressure to increase to the point where the soil particles can readily move with respect to each other. It may even become great enough to result in small geysers, called sand blows (Fig. 2), which eject water from the soil (Grant and others, 1998).

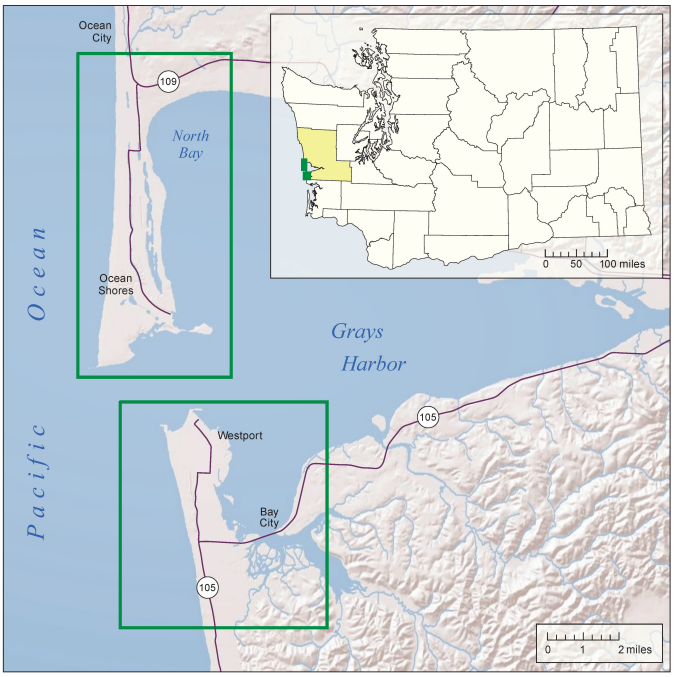

Figure 1. The green polygons delineate the approximate study areas on the Ocean Shores and Westport peninsulas. The inset map shows the location of Grays Harbor County (yellow polygon) and the map area (green boxes) relative to other counties in Washington State.

During a CSZ earthquake, liquefaction may occur in water-saturated sediment, causing damage to buildings, bridges, roadways, and other infrastructure. Geologic deposits recognized as susceptible to liquefaction include late Quaternary alluvial and fluvial sedimentary deposits and artificial fill (Palmer and others, 2002; Grant and others, 1998). Recent subduction zone earthquakes in Chile in 2010 (Fig. 3) and Japan in 2011 and crustal earthquakes in New Zealand 2010 and 2011 caused widespread liquefaction. In Chile, liquefaction was widespread but concentrated where sandy soils are prevalent in the southern part of the region affected by the earthquake. In Japan, liquefaction was also widespread, particularly in the Tokyo Bay region where artificial fill was placed on intertidal mud. Examples of historic liquefaction damage in Washington State are documented for three Puget Sound earthquakes: a M7.1 in the Olympia–Tacoma area on April 13, 1949; a M6.5 in the Seattle area on April 29, 1965 (Chleborad and Schuster, 1998); and the Nisqually earthquake, a M6.8 in the south Puget Sound area on February 26, 2001. These earthquakes resulted in significant damage to buildings, bridges, highways, railroads, water distribution systems, and marine facilities, with damage estimates from the 1949 and 1965 quakes totaling $25 million and $12 million, respectively (Grant and others, 1998), and more than $2 billion for the Nisqually earthquake (Highland, 2003).

Landslides

Correlations between earthquake magnitude and landslide distribution demonstrate that a M9+ earthquake can potentially trigger slope failures in an area exceeding 150,000 square miles (Keefer, 1984). However, accurately predicting which slopes will move and the severity of that movement is difficult (Jibson, 1993). This report analyzes two types of slope failures: shallow and deep-seated landslides. Generally, shallow landslides are those in which only the soil on the slope mobilizes. They can range in size from a few cubic yards to hundreds or thousands of cubic yards. Deep-seated landslides are those that initiate below the rooting depth of vegetation, commonly in bedrock, and tend to be larger than shallow landslides. They can, in extreme examples, be up to several miles in length.

Figure 2. Examples of seismically induced liquefaction damage to transportation networks in Olympia, Wash., and Christchurch, New Zealand. *Top left*. A large hole created by liquefaction on a paved road during the 2011 M6.3 Christchurch, New Zealand, earthquake. The hole was likely filled with silty water resulting from liquefaction when the car drove into the hole. Note the dried water line on the side of the car. Photo: Martin Luff. *Top right*. Deschutes Parkway in Olympia, Wash., after the 2001 M6.8 Nisqually earthquake. Photo: Bill Lingley. *Bottom left*. A buoyed storm drain passes through the pavement of a road during the 2011 M6.3 Christchurch, New Zealand, earthquake. Photo: Martin Luff. *Bottom right*. Sand blow from liquefaction spreads sediment and water across a residential road during the 2011 M6.3 Christchurch, New Zealand, earthquake. Photo: Martin Luff.

The slope stability analysis in this report is intended as an estimate of shallow landslide vulnerability for the entire report area. The analysis examines two shallow landslide conditions: (1) soils overlying bedrock and (2) dune sand with no underlying bedrock. Uniform soil values are used for each condition throughout the report area. We also calculate the vulnerability of deep-seated landslides in discrete areas with sufficient geotechnical data for estimating slope stability. This analysis does not account for weaknesses (fractures) or site-specific properties of bedrock, the various layers of different bedrock, or modification to the landscape (for example, cut slopes).

REGIONAL GEOLOGY AND PHYSIOGRAPHY

The report area lies in the Grays Harbor basin, south of the Olympic Range and east of the convergence of the North American tectonic plate and the subducting Juan de Fuca plate (Fig. 4). The mouth of the 91-square-mile basin is partially bounded on the west by the 7-mile-long Ocean Shores Peninsula in the north and 4-mile-long Westport Peninsula in the south (Fig. 1). The two peninsulas both average 1.5 miles wide. The remainder of the basin is

bounded by low-relief hills deeply incised by streams. The main stream that feeds into Grays Harbor is the Chehalis River, which enters the harbor on the east. The Chehalis River watershed is the second largest river drainage in Washington State and drains more than 2600 square miles (Ely and others, 2008) contained entirely in southwest Washington. The local geology of both peninsulas consists of unconsolidated sediments, largely dune and beach sand. The difference between dune and beach sand is the method of deposition, where dune sand is deposited by wind and beach sand is deposited by waves. Boreholes documented by Rau and McFarland (1982) indicate that the thickness of unconsolidated sediments in the area ranged from 900 to 1100 feet. The upland geology is different for both peninsulas. The uplands of the Ocean Shore peninsula consist of Pleistocene glacial outwash (Logan, 2003) that locally averages 50 to 60 feet above sea level. The uplands on the Westport peninsula are mapped as Quaternary terrace deposits (Logan, 1987); however, field observations and topographic maps suggest the geology may actually be deeply weathered siltstone and sandstone of the Lincoln Creek Formation, locally reaching elevations as much as 150 feet above sea level.

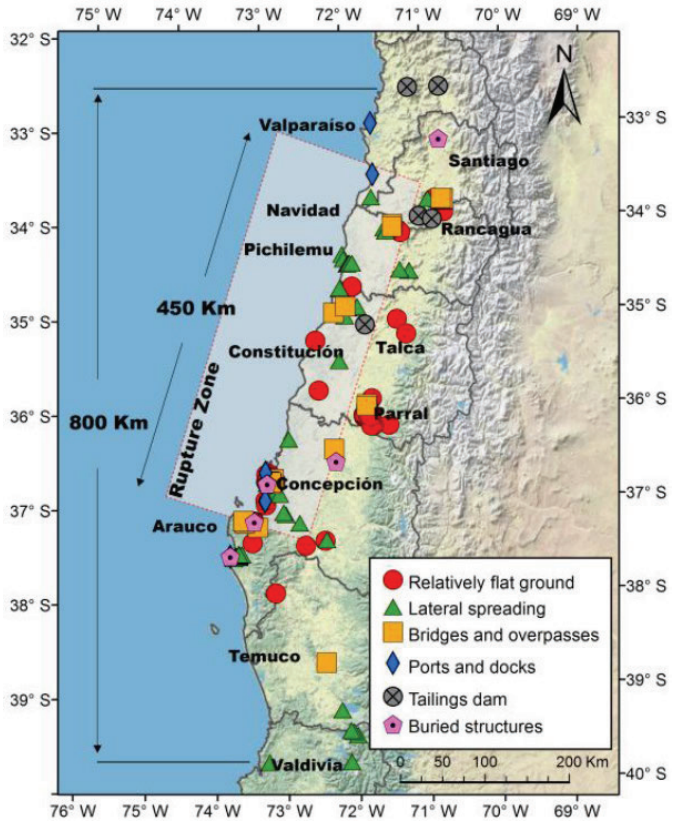

Figure 3. Documented liquefaction sites from the 2010 Chile M8.8 earthquake (Verdugo, 2012).

METHOD OF ANALYSIS

Our analysis of earthquake-induced shallow landslides follows methods originally developed by Newmark (1965) and modified by Jibson and others (1998), Romeo (2000), Capolongo and Refrice (2002), Harp and others (2006), Jibson (2007), and Miles and Keefer (2007). Our analysis of earthquake-induced soil liquefaction follows methods from Grant and others (1998), Palmer and others (1994, 2002, 2003), and Kramer (2008). Detailed descriptions of the methods used to model earthquake-induced landslides and soil liquefaction are given in Appendices A and B, respectively.

RESULTS AND DISCUSSION

Ground shaking during a M9+ CSZ earthquake can exceed 0.40 *g* on bedrock, and slopes with a critical acceleration of less than 0.40 *g* are considered vulnerable to seismically induced shallow landslides. The critical acceleration is the seismically induced ground acceleration at which the slope exceeds its static stability; a lower critical acceleration indicates a higher relative vulnerability to failure (Jibson and others, 1998, 2000). Slopes with a low critical acceleration (that is, less than 0.20 *g*) are the most vulnerable to shallow landslide initiation due to the likelihood that the slope will exceed the calculated critical acceleration during a CSZ event.

The spatial distribution of areas vulnerable to seismically induced shallow landslides associated with a M9+ CSZ earthquake is shown on Sheets 1 and 2. In order to better represent different groundwater scenarios, we analyzed two soil saturation conditions: Sheet 1 represents dry season conditions, such as summer and early autumn, and Sheet 2 represents wet winter conditions or an intense or prolonged precipitation event. Comparison of the two sheets shows the importance of groundwater to slope stability. Soil saturation decreases the forces resisting slope movement, which decreases the critical acceleration necessary to exceed the static stability of the slope and increases the likelihood of seismically induced slope movement. Soil dryness increases the forces resisting slope

movement, which increases the critical acceleration necessary to exceed the static stability of the slope and decreases the likelihood of seismically induced slope movement.

The shallow landslide hazard on the lowlands in the report area will likely consist of sand flows from steep dune faces. Clean dune sand has no cohesion, but beach grasses and other vegetation, including native shrubs and trees, increase the cohesion of the sand by root growth. Root cohesion is extremely difficult to quantify, and despite marginal increases in root cohesion, most dunes have some likelihood of seismically induced slope movement. If shallow landslides were to occur, the low elevation, moderate slope angles, and lack of cohesive sediments will prevent the landslides from mobilizing far beyond the break in slope at the base of the dune. This is not the case for shallow landslides from the uplands on the Westport peninsula, where cohesive soils with clay and silt can potentially mobilize and transport sediment a significant distance downslope. Structures and roads below a shallow upland landslide are likely to be damaged or blocked, due to the ability of cohesive landslides to effectively mobilize and transport debris, including trees, rocks, and soil, downslope. Where evacuation routes coincide with areas of increased shallow landslide vulnerability, there is potential for blockage due to sediment and debris on the road, as well as deformation or mobilization of the road grade itself.

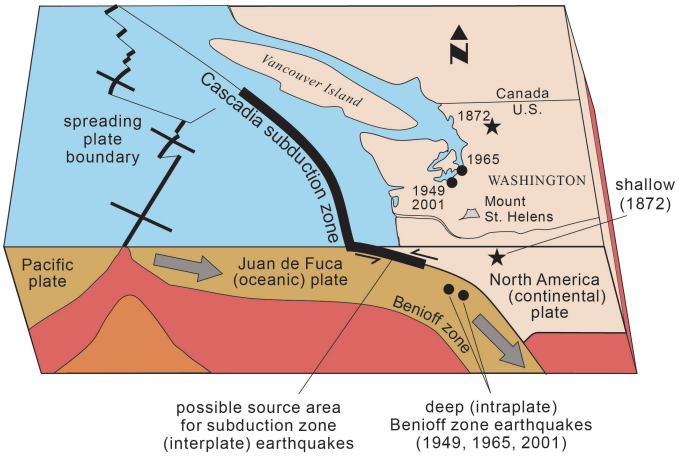

Figure 4. The Cascadia subduction zone (CSZ) at the boundary between the subducting Juan de Fuca plate and the North American plate. A CSZ earthquake could produce a M9+ earthquake (Satake and others, 2003) and peak ground accelerations on the Washington coast up to 0.40 *g* on bedrock, with shaking durations of up to several minutes (Art Frankel, U.S. Geological Survey, written commun., 2008). This level of ground acceleration is sufficient to initiate soil liquefaction and shallow landslides.

Deep-seated landslide analysis of the report area was not feasible due to an absence of detailed geotechnical data. Previous deep-seated landslide analysis performed in Aberdeen, Cosmopolis, and Hoquiam (Slaughter and others, 2013a), in geology similar to the uplands on the Westport peninsula, found the results over-predict the hazard of seismically induced, deep-seated landslide initiation. This was likely due to a lack of detailed rock information, which requires a site-specific analysis, typically including drilling rock cores and laboratory testing of samples—data not available for the study area. The absence of detailed rock-properties data for the peninsula forced us to forgo this analysis for the project area.

All of the beach, dune, and interdune sands on the Ocean Shores and Westport peninsula lowlands are *susceptible* to liquefaction. A soil considered susceptible to liquefaction is one that can liquefy under some level of loading, and a non-susceptible soil cannot liquefy—no matter how strong the loading may be (Kramer, 2008). However, further analysis is necessary to determine whether the shaking from a CSZ M9+ earthquake is strong enough to *initiate* liquefaction and create the ground failures associated with liquefaction. Evaluation of initiation of liquefaction for sites in the tsunami inundation zone (Fig. 5) and lowlands of the report area typically require analysis of geotechnical boreholes. We found only three reports documenting 29 boreholes (Sheet 3) in unconsolidated sediments for the Ocean Shores peninsula and found no borehole data for the Westport peninsula. The small borehole population was also very shallow, with 25 boreholes with an average depth of less than 10 feet. The remaining four[1] were WSDOT boreholes, all within 150 feet of each other, with an average depth exceeding 40 feet. Data for nine boreholes were input into the computer program WSliq.

Normally, sandy soils have the greatest likelihood of initiation of liquefaction, and these soils underlie much of the report area. However, analysis of the limited borehole data categorized the initiation of liquefaction hazard as very low to low, with only one borehole calculating as high. The low initiation of liquefaction values are likely due to compaction of sand by wave action from the Pacific Ocean and reflect similar results from the Long Beach peninsula (Slaughter and others, 2013b), where wave action compacted the sand on beaches to such a degree that the

[1] The four WSDOT boreholes were for a bridge project. Two boreholes were drilled 150 feet apart, and soils were sampled to a depth of approximately 75 feet. Six months later, WSDOT returned to the same location and drilled boreholes adjacent to the previous boreholes, this time sampling from approximately 75 feet to depths exceeding 115 feet. Because we are interested in only the upper 40 feet of a borehole, we analyzed the shallower two of the four boreholes.

seismic energy necessary to initiate liquefaction may not be strong enough to initiate widespread liquefaction. The sole Ocean Shores borehole to calculate as high was one of two WSDOT boreholes analyzed in the study area. The two boreholes are approximately 150 feet apart and located on opposite sides of the primary canal that divides the Ocean Shores peninsula (Plate 3). We consider WSDOT boreholes the highest quality due to excellent logs and a standard protocol that is consistent for all WSDOT boreholes in unconsolidated sediment. Unfortunately, the high variability in the liquefaction hazard calculation for the WSDOT borehole data is likely due to a difference in the interpretation and analysis of the borehole soil samples. The borehole with the high liquefaction rating (Appendix C, borehole WSDOT 17 TH-2-03) was characterized as consisting primarily of a clean sand (USCS SP) lacking silt, whereas the borehole with the adjacent low liquefaction rating (Appendix C, borehole WSDOT 17 TH-1-03) was characterized as primarily sand with a small percentage of silt (USCS SP-SM). This difference in silt content is sufficient to change the liquefaction hazard rating. We find that the general lack of borehole data across the two peninsulas makes extrapolation of initiation of liquefaction hazard assessment difficult. Instead, liquefaction analysis will follow mapping techniques similar to those used in our report for the Long Beach peninsula (Slaughter and others, 2013b), where we opted to use soil mapping as our primary data source for liquefaction.

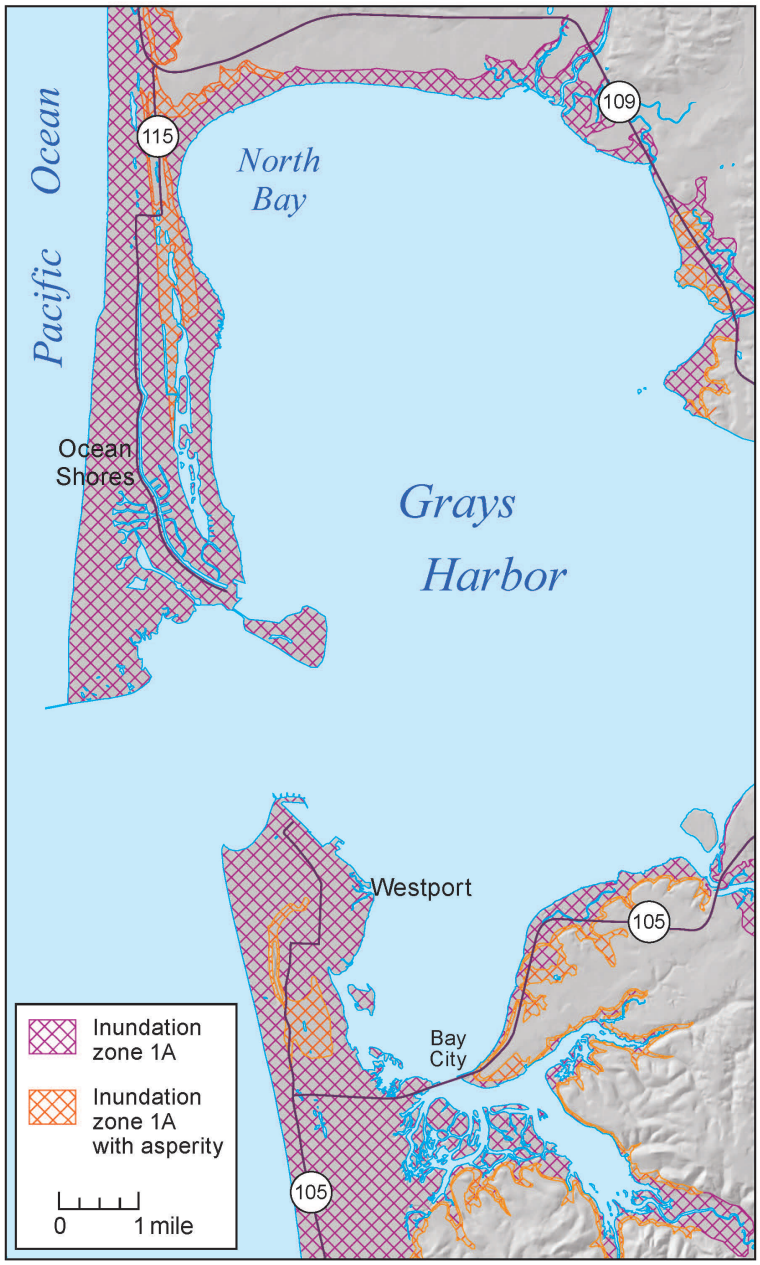

Figure 5. Tsunami inundation zones for a tsunami initiated by a M9+ Cascadia subduction zone earthquake on the Ocean Shores and Westport peninsulas. Hatch and cross-hatch patterns represent different inundation zones from a CSZ earthquake, which are described in Walsh and others (2000).

At the Long Beach peninsula, it was estimated that interdune sand, the low-elevation sand between sand dunes, is more vulnerable to initiation of liquefaction than dune sand, due to the proximity of groundwater and the increased likelihood that interdune sand may be saturated. The situation is similar for both the Westport and Ocean Shores peninsulas. However, when compared to the Westport peninsula, the Ocean Shores peninsula may have a slightly reduced liquefaction hazard, due to the numerous artificial ponds and canals, which have likely lowered the water table in nearby areas. Lateral spreading, a form of liquefaction where a soil deforms horizontally (see top right image in Fig. 2), may be an increased hazard in areas adjacent to artificial ponds and canals that have been excavated and contain a free face where deformation could occur.

There are no areas previously mapped as artificial fill; however, analysis of historic USGS mapping identified potential artificial fill at Westhaven Cove on the Westport peninsula. Though the area appears to lack detailed construction records, a draft environmental assessment (U.S. Army Corps of Engineers, 2013) describes a brief

history of Westhaven Cove, home to a large commercial fishing fleet. The U.S. Army Corps of Engineers enlarged the harbor in the 1950s, and it is likely that the waterfront area was filled in with dredge materials excavated to create the harbor, as was done in other harbor projects, such as Ilwaco. Dredge fills were typically applied without regard to engineering properties or application technique, creating soils potentially very vulnerable to initiation of liquefaction. The liquefaction hazard for the port is difficult to quantify because of the high variability of the soil properties of fill and lack of subsurface data. However, historic evidence of fills that experienced seismic shaking, such as from the M6.5 1965 Seattle area event or the 2001 Nisqually earthquake, reported significant initiation of liquefaction of non-engineered fills, and we consider all documented or suspected non-engineered fill as highly vulnerable to initiation of liquefaction.

Peat is a significant deposit and underlies a minimum of 987 acres (781acres on the Ocean Shore Peninsula and 206 acres on the Westport peninsula) or approximately 7 percent of the total area of the lowlands. Peat, which is not liquefiable, is still considered at risk for deformation and sand boils from underlying liquefiable sediments. The mapped acreage of peat deposits may be significantly larger with the recent addition of a wetlands database to the National Wetlands Inventory (U.S. Fish and Wildlife Service, 2012). This reconnaissance dataset identified 1317 acres of wetlands on the Ocean Shores peninsula (14% of the peninsula) and 951 acres on the Westport peninsula (18% of the peninsula, not including the uplands). Nearly all of the mapped peat deposits coincide with the wetlands inventory; however, not all of the wetlands contain peat. Wetlands should be considered areas where saturated soils are present in the subsurface and there is an increased likelihood of initiation of liquefaction, as well as potential hazards from unmapped peat deposits. Tsunami evacuation routes on both the Ocean Shores and Westport peninsulas cross at least one peat deposit or wetland (Sheet 3), and any place an evacuation route crosses a mapped peat deposit or wetland, there is a risk of seismically induced deformation of the roadway.

The area subject to the initiation of earthquake-induced soil liquefaction from ground shaking associated with a M9+ CSZ earthquake includes much of the Ocean Shores and Westport peninsulas and their mapped tsunami inundation zones (Sheet 3). Unfortunately, lack of borehole data for the peninsulas requires broad assumptions of initiation of liquefaction, based primarily on soils, lidar DEM, and wetlands mapping. Our interpretation of the overall initiation of liquefaction hazard on the peninsula is low to moderate, with deformation of peat a significant potential hazard. Areas with wetlands may be more vulnerable to initiation of liquefaction, due to the availability of groundwater in unconsolidated sediments. Moderate liquefaction hazards are associated with low-elevation interdune sands, where sediments were not compacted by wave action and may have groundwater near the subsurface. This may be especially true where interdune sands coincide with wetlands, and sediments may be saturated. The only area of high hazard is the Westhaven Cove waterfront, where artificial fill consisting of dredge materials from the excavation of the port is likely very vulnerable to initiation of liquefaction.

RECOMMENDATIONS

This report evaluates the vulnerability to initiation of soil liquefaction and shallow landslides from a Cascadia subduction zone (CSZ) earthquake for the Ocean Shores and Westport peninsulas in Grays Harbor County, Washington. The objective is to assist city and emergency management officials in evaluating the suitability of existing evacuation routes and to suggest potential modifications of routes and assembly areas based on vulnerability to ground failure during a M9+ CSZ earthquake. If existing evacuation routes are found to be problematic, there are several potential mitigation techniques to revitalize the evacuation route network. Recommendations include:

- **Add walking evacuation routes.** In the event of a CSZ earthquake, there is potential for ground failures from liquefaction and shallow landslides as well as deformation of peat. These may result in damaged buildings, downed utility lines, and buckled roads that could make some transportation networks impassable to vehicles, forcing people to evacuate on foot. Adding walking evacuation routes may also require adding evacuation assembly areas.
- **Create a disaster-resistant population.** Prepare citizens for the potential earthquake-induced damage and provide advice on evacuation when ground failure has occurred. Workshops, flyers, and community evacuation practice are examples of dissemination of information and guidance. Annual participation in the shakeout.org earthquake drills [http://www.shakeout.org/washington/], including citizens following tsunami evacuation routes to assembly areas are excellent techniques to educate and reinforce earthquake preparedness.
- **Consider stabilization of evacuation routes at risk.** If a driving evacuation route is the only method of evacuation and the route is vulnerable to initiation of liquefaction, stabilization of the subsurface to harden the

evacuation routes can reduce the vulnerability to initiation of liquefaction. This is an expensive alternative, but may be necessary when long distances must be traveled in a short time to attain high ground.

- **Future work.** This is an initial overview of liquefaction hazards on the Ocean Shores and Westport peninsulas. Future analysis should include a detailed borehole or cone penetrometer analysis along existing and planned evacuation routes, as well as when constructing critical infrastructure. More borehole data are necessary to better understand the seismic response of the peninsulas and to better calculate potential ground failure hazards related to a CSZ event.

Knowledge of the location of potential ground failures will provide city officials and emergency managers with information regarding the potential seismic risks citizens face after a CSZ M9+ earthquake. Careful and creative review of evacuation routes and areas of potential ground failure may indicate more appropriate routes and modes of transportation for tsunami evacuation.

ACKNOWLEDGMENTS

We would like to thank WADGER staff Anne Olson, Ian Hubert, and Jari Roloff for cartography, editing, and manuscript preparation. Also thanks to all the staff at Ocean Shores, GeoEngineers, and Grays Harbor County who shared their offices and time to provide borehole logs, geotechnical reports, and other data critical to this report.

REFERENCES CITED

Boulanger, R. W.; Idriss, I. M., 2004, Evaluating the potential for liquefaction or cyclic failure of silts and clays: Report UCD/CGM-04/01, Center for Geotechnical Modeling, University of California [Davis, CA], 130 p. [link to PDF on Google.com]

Boulanger, R. W.; Idriss, I. M., 2005, Evaluating cyclic failure in silts and clays; Proceedings, Geotechnical Earthquake Engineering Satellite Conference on Performance Based Design in Earthquake Geotechnical Engineering: Concepts and Research: Prepared by TC4 Committee of ICSMGE, Japanese Geotechnical Society [Tokyo], p. 78-86. [http://www.geologi.emilia-romagna.it/pwd/download/Mat_bibliogr_2.pdf]

Bray, J. D.; Sancio, R. B., 2006, Assessment of the liquefaction susceptibility of fine-grained soils: Journal of Geotechnical and Geoenvironmental Engineering, v. 132, no. 9, p. 1165-1177.

Buchanan, P. N.; Savigny, K. W., 1990, Factors controlling debris avalanche initiation: Canadian Geotechnical Journal, v. 27, no. 5, p. 659-675.

Cakir, Recep; Walsh, T. J., 2012, Shallow seismic site characterizations at 25 ANSS/PNSN stations and compilation of site-specific data for the entire strongmotion network in Washington and Oregon: U.S. Geological Survey, External research support—Final technical reports—Funded research, Pacific Northwest, 56 p. [http://earthquake.usgs.gov/research/external/reports/G11AP20045.pdf]

Capolongo, Domenico; Refice, Alberto, 2002, Probabilistic modeling of uncertainties in earthquake-induced landslide hazard assessment: Computers and Geoscience, v. 28, p. 735-749.

Cetin, K. O.; Seed, R. B.; Der Kiureghian, Armen; Tokimatsu, Kohji; Harder, L. F.; Kayen, R. E.; Moss, R. E. S., 2004, Standard penetration test-based probabilistic and deterministic assessment of seismic soil liquefaction potential: Journal of Geotechnical and Geoenvironmental Engineering, v. 130, no. 12, p. 1314-1340. [http://tinyurl.com/arl5acm]

Chleborad, A. F.; Schuster, R. L., 1998, Ground failure associated with the Puget Sound region earthquakes of April 13, 1949, and April 29, 1965. *In* Rogers, A. M.; Walsh, T. J.; Kockelman, W. J.; Priest, G. R., editors, Assessing earthquake hazards and reducing risk in the Pacific Northwest: U.S. Geological Survey Professional Paper 1560, v. 2, p. 373-440. [http://pubs.usgs.gov/pp/p1560/p1560po.pdf]

Earthquake Engineering Research Institute, 2005, EERI special earthquake report—January 2005; Preliminary observations on the Niigata Ken Chuetsu, Japan, earthquake of October 23, 2004: Earthquake Engineering Research Institute, 12 p. [http://www.eeri.org/lfe/pdf/japan_niigata_eeri_preliminary_report.pdf]

Ely, D. M.; Frasl, K. E.; Marshall, C. A.; Reed, Fred, 2008, Seepage investigation for selected river reaches in the Chehalis River basin, Washington: U.S. Geological Survey Scientific Investigations Report 2008-5180, 12 p. [http://pubs.usgs.gov/sir/2008/5180/]

Gorum, T.; Fan, X.; van Westen, C. J.; Huang, R. Q.; Xu, Q.; Tang, C.; Wang, G., 2011, Distribution pattern of earthquake-induced landslides triggered by the 12 May 2008 Wenchuan earthquake: Geomorphology, v. 133, no. 3-4, p. 152-167.

Grant, W. P.; Perkins, W. J.; Youd, T. L., 1998, Evaluation of liquefaction potential in Seattle, Washington. *In* Rogers, A. M.; Walsh, T. J.; Kockelman, W. J.; Priest, G. R., editors, Assessing earthquake hazards and reducing risk in the Pacific Northwest: U.S. Geological Survey Professional Paper 1560, v. 2, p. 441-473, 1 plate. [http://pubs.usgs.gov/pp/p1560/p1560po.pdf]

Hancox, Graham; Perrin, Nick; Van Dissen, Russ, 2011, Report on landslide reconnaissance flight on 24 February 2011 following the MW 6.3 Christchurch earthquake of 22 February 2011: GNS Science, 44 p. [http://info.geonet.org.nz/ download/attachments/2196288/Christchurch_response.pdf]

Harp, E. L.; Jibson, R. W., 1996, Landslide triggered by the 1994 Northridge, California, earthquake: Bulletin of the Seismological Society of America, v. 86, no. 1B, p. S319-S332.

Harp, E. L.; Michael, J. A.; Laprade, W. T., 2006, Shallow-landslide hazard map of Seattle, Washington: U.S. Geological Survey Open-File Report 2006-1139, 18 p., 2 plates, scale 1:25,000. [http://pubs.usgs.gov/of/2006/1139/]

Highland, L. M., 2003, An account of preliminary landslide damage and losses resulting from the February 28, 2001, Nisqually, Washington, earthquake: U.S. Geological Survey Open-File Report 03-211, version 1.1, 48 p. [http://pubs.usgs.gov/of/2003/ofr-03-211/]

Idriss, I. M.; Boulanger, R. W., 2008, Soil liquefaction during earthquakes: Earthquake Engineering Research Institute MNO-12, 237 p.

Ilwaco Tribune, 1949, No damage here as quake rocks Pacific Northwest: Ilwaco Tribune, April 15, 1949, no. 15, cover page.

Jibson, R. W., 1993, Predicting earthquake-induced landslide displacements using Newmark's sliding block analysis: Transportation Research Record, no. 1411, p. 9-17.

Jibson, R. W., 2007, Regression models for estimating coseismic landslide displacement: Engineering Geology, v. 91, no. 2-4, p. 209-218.

Jibson, R. W.; Harp, E. L.; Michael, J. A., 1998, A method for producing digital probabilistic seismic landslide hazard maps—An example from the Los Angeles, California, area: U.S. Geological Survey Open-File Report 98-113, 17 p., 2 plates. [http://pubs.usgs.gov/of/1998/ofr-98-113/]

Jibson, R. W.; Harp, E. L.; Michael, J. A., 2000, A method for producing digital probabilistic seismic landslide hazard maps: Engineering Geology, v. 58, p. 271-289. [http://tinyurl.com/a4jrc2y]

Keefer, D. K., 1984, Landslides caused by earthquakes: Geological Society of America Bulletin, v. 95, no. 4, p. 406-421.

Kieffer, D. S.; Jibson, R. W.; Rathje, E. M.; Kelson, Keith, 2006, Landslide triggered by the 2004 Niigata Ken Chuetsu, Japan, earthquake: Earthquake Spectra, v. 22, no. S1, p. S47-S73. [http://tinyurl.com/ab9lk8s]

Koloski, J. W.; Schwarz, S. D.; Tubbs, D. W., 1989, Geotechnical properties of geologic materials. *In* Galster, R. W., chairman, Engineering geology in Washington: Washington Division of Geology and Earth Resources Bulletin 78, v. I, p. 19-26. [http://www.dnr.wa.gov/publications/ger_b78_engineering_geol_v1_pt1of5.pdf]

Kramer, S. L., 2008, Evaluation of liquefaction hazards in Washington State: Washington State Transportation Center (TRAC), Research Report WA-RD 668.1, 1 v. [http://www.wsdot.wa.gov/research/reports/600/668.1.htm]

Logan, R. L., compiler, 1987, Geologic map of the Chehalis River and Westport quadrangles, Washington: Washington Division of Geology and Earth Resources Open File Report 87-8, 16 p., 1 plate, scale 1:100,000. [http://www.dnr.wa.gov/publications/ger_ofr87-8_geol_map_chehalisriver_westport_100k.zip]

Logan, R. L., compiler, 2003, Geologic map of the Copalis Beach 100,000 quadrangle, Washington: Washington Division of Geology and Earth Resources Open File Report 2003-16, 1 plate, scale 1:100,000. [http://www.dnr.wa.gov/publications/ger_ofr2003-16_geol_map_copalisbeach_100k.zip]

Mayne, P. W.; Christopher, B. R.; DeJong, Jason, 2001, Manual on subsurface investigations—Geotechnical site characterization: National Highway Institute Publication FHWA NHI-01-031, 1 v. [http://www.geotechnicaldirectory.com/publications/manuals/NHI_SI_Manual.pdf]

Miles, S. B.; Keefer, D. K., 2007, Comprehensive areal model of earthquake-induced landslides—Technical specification and user guide: U.S. Geological Survey Open-File Report 2007-1072, 69 p. [http://pubs.usgs.gov/ of/2007/1072/]

Newmark, N. M., 1965, Effects of earthquakes on dams and embankments: Geotechnique, v. 15, no. 2, p. 139-160.

Palmer, S. P.; Evans, B. D.; Schasse, H. W., 2002, Liquefaction susceptibility of the Greater Eastside area, King County, Washington: Washington Division of Geology and Earth Resources Geologic Map GM-48, 1 sheet, scale 1:36,000, with 14 p. text. [http://www.dnr.wa.gov/publications/ger_gm48_liquefaction_suscep_eastside_ area.zip]

Palmer, S. P.; Magsino, S. L.; Bilderback, E. L.; Poelstra, J. L.; Folger, D. S.; Niggemann, R. A., 2004, Liquefaction susceptibility and site class maps of Washington State, by county: Washington Division of Geology and Earth Resources Open File Report 2004-20, 78 plates, 45 p. text. [http://www.dnr.wa.gov/ResearchScience/Topics/GeologyPublicationsLibrary/Pages/pub_ofr04-20.aspx]

Palmer, S. P.; Moses, L. J., 1996, Ground failures caused by the Robinson Point earthquake, southern Puget Sound region, Washington [abstract]: Geological Society of America Abstracts with Programs, v. 28, no. 5, p. 98.

Palmer, S. P.; Perkins, W. J.; Grant, W. P., 2003, Liquefaction susceptibility of the greater Tacoma urban area, Pierce and King Counties, Washington: Washington Division of Geology and Earth Resources Geologic Map GM-51, 1 sheet, scale 1:30,000 with 11 p. text. [http://www.dnr.wa.gov/publications/ger_gm51_liquefaction_ suscep_tacoma_area.zip]

Palmer, S. P.; Schasse, H. W.; Norman, D. K., 1994, Liquefaction susceptibility for the Des Moines and Renton 7.5-minute quadrangles, Washington: Washington Division of Geology and Earth Resources Geologic Map GM-41, 2 sheets, scale 1:24,000, with 15 p. text. [http://www.dnr.wa.gov/publications/ger_gm41_liquifaction_suscep_ desmoines_renton_area.pdf]

Pringle, R. F., 1986, Soil survey of Grays Harbor County area, Pacific County, and Wahkiakum County, Washington: U.S. Soil Conservation Service, 296 p., 165 plates.

Rau, W. W.; McFarland, C. R., 1982, Coastal wells of Washington: Washington Division of Geology and Earth Resources Report of Investigations 26, 4 sheets. [http://www.dnr.wa.gov/publications/ger_ri26_coastal_wells_wa.pdf]

Romeo, Roberto, 2000, Seismically induced landslide displacements—A predictive model: Engineering Geology, v. 58, no. 3-4, p. 337-351.

Satake, Kenji; Wang, Kelin; Atwater, B. F., 2003, Fault slip and seismic moment of the 1700 Cascadia earthquake inferred from Japanese tsunami description: Journal of Geophysical Research, v. 108, no. B11, 2535, DOI:10.1029/2003JB002521, p. ESE 7-1 - 7-17.

Schulz, W. H.; Galloway, S. L.; Higgins, J. D., 2012, Evidence for earthquake triggering of large landslides in coastal Oregon, USA: Geomorphology, v. 141-142, p. 88-98.

Seed, H. B.; Idriss, I. M., 1982, Ground motions and soil liquefaction during earthquakes: Earthquake Engineering Research Institute, 134 p.

Seed, R. B.; Cetin, K. O.; Moss, R. E. S.; Kammerer, A. M.; Wu, J.; Pestana, J. M.; Riemer, M. F.; Sancio, R. B.; Bray, J. D.; Kayen, R. E.; Faris, A., 2003, Recent advances in soil liquefaction engineering—A unified and consistent framework: 26th Annual ASCE Los Angeles Geotechnical Spring Seminar, Keynote Presentation, H.M.S. Queen Mary [Long Beach, CA], Report no. EERC 2003-06, 71 p. [http://tinyurl.com/a9pek7m]

Slaughter, S. L.; Walsh, T. J.; Ypma, Anton; Stanton, K. M. D.; Cakir, Recep; Contreras, T. A., 2013a, Earthquake-induced landslide and liquefaction susceptibility and initiation potential maps for tsunami inundation zones in Aberdeen, Hoquiam, and Cosmopolis, Grays Harbor County, Washington, for a M9+ Cascadia subduction zone event: Washington Division of Geology and Earth Resources Report of Investigations 36, 2 sheets with 39 p. text. [http://www.dnr.wa.gov/publications/ger_ri36_aberdeen_liquefaction.zip]

Slaughter, S. L.; Walsh, T. J.; Ypma, Anton; Stanton, K. M. D.; Cakir, Recep; Contreras, T. A., 2013b, Landslide and liquefaction maps for the Long Beach peninsula, Pacific County, Washington—Effects on tsunami inundation zones of a Cascadia subduction zone earthquake: Washington Division of Geology and Earth Resources Report of Investigations 37, 2 sheets with 35 p. text. [http://www.dnr.wa.gov/publications/ger_ ri37_longbeach_liquefaction.zip]

Thomas, B. E., 1995, Ground-water flow and water quality in the sand aquifer of Long Beach peninsula, Washington: U.S. Geological Survey Water-Resources Investigations Report 95-4026, 168 p.

Transportation Research Board, 2001, Guide for mechanistic-empirical design of new and rehabilitated pavement structures; appendix CC, 204 p. [http://onlinepubs.trb.org/onlinepubs/archive/mepdg/2appendices_cc.pdf]

U.S. Army Corps of Engineers, 2013, Draft Environmental Assessment Fiscal Years 2013 through 2020 Point Chehalis Revetment Maintenance Project Westport, Grays Harbor County, Washington, April 2013, 64 p. [http://www.nws.usace.army.mil/Portals/27/docs/environmental/resources/2013%20Environmental%20Documents/2013%20-%20Draft%20EA%20FY13-20%20Point%20Chehalis%20Revetment%20Maintenance.pdf]

U.S. Army Corps of Engineers, 2003, Engineering and design—Slope stability: Engineer Manual EM 1102-2-1902, 205 p. [http://publications.usace.army.mil/publications/eng-manuals/EM_1110-2-1902_sec/EM_1110-2-1902.pdf]

U.S. Bureau of Reclamation, 1998, Engineering geology field manual; 2d ed., Volume 1: U.S. Bureau of Reclamation, 478 p. [http://www.usbr.gov/pmts/geology/].

U.S. Fish and Wildlife Service, 2012, National Wetlands Inventory [webpage]: U.S. Fish and Wildlife Service. [accessed January 5, 2013, at http://www.fws.gov/wetlands/]

U.S. Geological Survey, 2011, Peak ground acceleration [GIS data]: U.S. Geological Survey. [accessed on Feb. 22, 2012, at http://earthquake.usgs.gov/earthquakes/shakemap/global/shake/Casc9.0_expanded_se/#Peak_Ground_ Acceleration]

Verdugo, Ramón, 2012, Comparing liquefaction phenomena observed during the 2010 Maule, Chile earthquake and 2011 Great East Japan earthquake. *In* Proceedings of the International Symposium on Engineering Lessons Learned from the 2011 Great East Japan Earthquake, March 1–4, 2012, Tokyo, Japan, p. 707-718. [http://www.jaee.gr.jp/event/seminar2012/eqsympo/pdf/papers/167.pdf]

Walsh, T. J.; Palmer, S. P., 1996, The 1995 Robinson Point earthquake, Puget Sound, Washington—A small event with potentially large consequences. *In* Bausch, Doug, compiler, WSSPC '95—Annual report and sixteenth meeting of the Western States Seismic Policy Council: Arizona Division of Emergency Management, p. 125.

Walsh, T. J.; Caruthers, C. G.; Heinitz, A. C.; Myers, E. P., III; Baptista, A. M.; Erdakos, G. B.; Kamphaus, R. A., 2000, Tsunami hazard map of the southern Washington coast—Modeled tsunami inundation from a Cascadia subduction zone earthquake: Washington Division of Geology and Earth Resources Geologic Map GM-49, 1 sheet, scale 1:100,000, with 12 p. text. [http://www.dnr.wa.gov/publications/ger_gm49_tsunami_hazard_ southern_coast.zip]

Walsh, T. J.; Myers, E. P., III; Baptista, A. M., 2002a, Tsunami inundation map of the Port Angeles, Washington, area: Washington Division of Geology and Earth Resources Open File Report 2002-1, 1 sheet, scale 1:24,000. [http://www.dnr.wa.gov/publications/ger_ofr2002-1_tsunami_hazard_portangeles.pdf]

Walsh, T. J.; Myers, E. P., III; Baptista, A. M., 2002b, Tsunami inundation map of the Port Townsend, Washington, area: Washington Division of Geology and Earth Resources Open File Report 2002-1, 1 sheet, scale 1:24,000. [http://www.dnr.wa.gov/publications/ger_ofr2002-1_tsunami_hazard_portangeles.pdf]

Walsh, T. J.; Myers, E. P., III; Baptista, A. M., 2003, Tsunami inundation map of the Neah Bay, Washington, area: Washington Division of Geology and Earth Resources Open File Report 2003-2, 1 sheet, scale 1:24,000. [http://www.dnr.wa.gov/publications/ger_ofr2003-2_tsunami_hazard_neahbay.pdf]

Walsh, T. J.; Titov, V. V.; Venturato, A. J.; Mofjeld, H. O.; Gonzalez, F. I., 2005, Tsunami hazard map of the Anacortes–Whidbey Island area, Washington—Modeled tsunami inundation from a Cascadia subduction zone earthquake: Washington Division of Geology and Earth Resources Open File Report 2005-1, 1 sheet, scale 1:62,500. [http://www.dnr.wa.gov/publications/ger_ofr2005-1_tsunami_hazard_anacortes_whidbey.pdf]

Washington Division of Geology and Earth Resources, 2007a, Tsunami! Evacuation map for Ocean Shores and vicinity: Washington Department of Natural Resources, Division of Geology and Earth Resources, 1 sheet. [http://www.dnr.wa.gov/publications/ger_tsunami_evac_oceanshores.pdf]

Washington Division of Geology and Earth Resources, 2007b, Tsunami! Evacuation map for Westport, Grayland, and Ocosta: Washington Department of Natural Resources, Division of Geology and Earth Resources, 1 sheet. [http://www.dnr.wa.gov/publications/ger_tsunami_evac_westport.pdf]

Washington Division of Geology and Earth Resources, 2012, Washington State Geologic Information Portal: Washington Division of Geology and Earth Resources online media. [http://www.dnr.wa.gov/geologyportal]

Washington State Department of Transportation, 2012, Geotechnical design manual, M46-03: Washington State Department of Transportation, 828 p. [http://www.wsdot.wa.gov/publications/manuals/M46-03.htm]

Watershed Sciences, Inc., 2010, Lidar remote sensing data collection—Southwest Washington: submitted to the Oregon Department of Geology and Mineral Industries (May 24, 2010), 1–25, available from Puget Sound Lidar Consortium. [http://pugetsoundlidar.ess.washington.edu/lidardata/restricted/nonpslc/swwash2009/swwash2009.html]

Youd, T. L.; Idriss, I. M.; Andrus, R. D.; Arango, Ignacio; Castro, Gonzalo; Christian, J. T; Dobry, Richardo; Liam Finn, W. D.; Harder, L. F., Jr.; Hynes, M. E.; Ishihara, Kenji; Koester, J. P.; Liao, S. S. C.; Marcuson, W. F., III; Martin, G. R; Mitchell, J. K.; Moriwaki, Yoshiharu; Power, M. S.; Robertson, P. K.; Seed, R. B.; Stokoe, K. H., II, 2001, Liquefaction resistance of soils; Summary report from the 1996 NCEER and 1998 NCEER/NSF Workshops on Evaluation of Liquefaction Resistance of Soils: Journal of Geotechnical and Geoenvironmental Engineering, v. 124, no. 10, p. 817-833.

Appendix A. Technical Description of Landslide Vulnerability Modeling from a Cascadia Subduction Zone M9+ Earthquake

INTRODUCTION

Large or prolonged ground motions from a Cascadia subduction zone (CSZ) magnitude 9+ (M9+) earthquake could trigger thousands of landslides throughout much of the affected area. In many cases, seismically induced landslides account for a significant portion of total earthquake damage (Jibson, 2007). Severe and prolonged ground shaking from a CSZ M9+ earthquake could persist for up to several minutes (Art Frankel, U.S. Geological Survey, written commun., 2008) and could initiate hundreds to thousands of landslides. On the Washington coast, landslides may prevent efficient evacuation from an impending tsunami and impede post-tsunami rescue efforts. Although tsunami inundation zones have been modeled and evacuation routes planned (Walsh and others, 2000; WADGER, 2007a,b), there have been no detailed evaluations of seismically induced landslide risk for evacuation routes in coastal communities. This appendix describes the technical background associated with the evaluation of landslide initiation for the Ocean Shores and Westport peninsulas, Grays Harbor County, Washington. The results of this analysis are intended to produce a preliminary screening tool for identifying areas vulnerable to seismically induced landslides.

This map is intended as a regional planning tool and is not intended for site-specific analysis. The maps included in this report cannot be used to determine landslide vulnerability in any specific locality. The maps included in this report cannot be substituted for a site-specific geotechnical investigation, which must be performed by qualified practitioners and is required to assess the potential for ground failures and consequent damage at a given locality.

BACKGROUND

Seismically induced landslides are a common occurrence during large-magnitude earthquakes. Correlations between earthquake magnitude and landslide distribution demonstrate that a M9+ earthquake can trigger slope failures in an area exceeding 150,000 square miles (Keefer, 1984). A detailed study of the 1994 Northridge, California, M6.7 earthquake found more than 11,000 landslides triggered in an area of approximately 3800 square miles (Harp and Jibson, 1996). A detailed remote reconnaissance of more than 13,500 square miles of the 2008 Wenchuan, China, M8.0 earthquake found more than 60,000 landslides (Gorum and others, 2011). A one-day reconnaissance of the 2011 Christchurch, New Zealand, M6.3 earthquake found 170 landslides triggered in an area of less than 60 square miles (Hancox and others, 2011). During the 2004 Niigata Ken Chuetsu, Japan, M6.6 earthquake, a minimum of 442 landslides occurred (EERI, 2005). Analysis of 40 historic earthquakes ranging from M5.1 to M9+ identified 14 different seismically induced landslide types that include both shallow and deep-seated landslide processes (Keefer, 1984). Examples from the 2004 Niigata Ken Chuetsu earthquake reveal that seismically triggered failure mechanisms comprise a broad spectrum of landslides, including shallow translational and deep-seated failures, large rock slides, slump-flow complexes, and debris flows (Kieffer and others, 2006).

Seismically induced shallow landslide vulnerability has been evaluated by the application of models in a geographic information system (GIS). Previous studies measured shallow landslide vulnerability and the seismic shaking to which the slope will be subjected (Capolongo and Refice, 2002; Jibson and others, 1998, 2000). Assessment of shallow landslide vulnerability is relatively simple; however, assessment of seismic shaking of a CSZ M9+ earthquake is complicated. Using Newmark's method (Newmark, 1965), the primary challenge of assessing seismic shaking is a complete lack of strong-motion data for a CSZ M9+ earthquake, and without this data, significant assumptions must be made. These assumptions are outside of the scope of this project, so we have opted to exclude seismic slope performance and instead focus on the dynamic stability of slopes in the report area. We will discuss Newmark's method later in this appendix.

The method used to evaluate slope stability is the critical acceleration (a_c), which is a measure of the dynamic stability of a soil on a slope and is compared to the seismically induced peak ground accelerations (PGA)(USGS, 2011) to which the slope will be subjected. If the PGA exceeds the a_c, the ground acceleration overcomes the basal sliding resistance of the soil to potentially initiate downslope movement (Jibson, 2007). However, Jibson (1993)

states that in cases where PGA exceeds the a_c, the a_c has proven to be vastly over-conservative because many slopes experience temporary earthquake accelerations well above their a_c but experience little or no permanent displacement. The reason for this is that the PGA may be experienced for only a few cycles of shaking, not long enough to trigger slope movement. We acknowledge this limitation regarding our analysis and consider an over-conservative analysis acceptable in regard to the evaluation of tsunami evacuation routes. If an evacuation route is required to pass under slopes identified as potentially unstable, it is highly advisable to call in an engineering geologist or geotechnical engineer for a site-specific analysis.

METHODS

This report includes two hazard maps delineating areas vulnerable to shallow landslide initiation. Construction of the hazard maps required several datasets, including soils mapping, soils property data, geologic mapping, and a lidar (light detection and ranging) digital elevation model (DEM). The evaluation of shallow landslides requires different modeling techniques for beach and dune sands in the lowlands and soils derived from bedrock in the uplands. The different modeling techniques and datasets used for each technique are discussed below.

Topography

We used a 3-foot-grid lidar DEM (Watershed Sciences Inc., 2010) and resampled the data to a 10-foot grid. Resampling was necessary to eliminate erroneous peaks and valleys in the original data, yet preserve the subtle topographic features where shallow landslides are likely to occur. Datasets derived from the DEM include slope gradient, hillshade, and slope profiles, all generated from ESRI ArcGIS 10, commercially available GIS software.

Geology and Soils

The geology of the area was compiled into 1:100,000-scale maps (Logan, 1987, 2003), so digital geologic and 1:6000-scale agricultural soil (Pringle, 1986) feature classes were superimposed to create a higher-resolution geologic map of the report area. The resulting map was then compared to a lidar DEM hillshade to demarcate the unconsolidated sediments of the lowlands from the bedrock geology of the uplands. The mosaicked surficial geology map was divided into units, based on geologic parent material and soils classified by the Unified Soil Classification System (USCS), and digitized in a GIS. Soil[2] property values, including cohesion, angle of internal friction, and unit weight, were acquired from geotechnical borehole logs from the area and other areas with similar geology, as well as various local and national sources (Harp and others, 2006; Koloski and others, 1989; Washington State Department of Transportation [WSDOT], 2012, and unpub. documents, 2000, 1998, 1997, 1995). Soil properties were assigned to the digitized USCS soil feature class as tabular data; feature classes were converted to a grid for efficient analysis.

Due to the differences in soil properties between dune sand in the lowlands and the bedrock-derived soils in the uplands, we used different material properties for each analysis. For the upland soils, we assumed that the shallow-landslide failure plane would occur on the bedrock and soil interface. Soil depth, which is shown on the 1:6000-scale agricultural soil maps, exceeds 60 inches over bedrock in much of the area. Our local knowledge of the upland soils and geology suggests that 60 inches is a conservative thickness and likely under-represents the actual soil thickness. Based on our interpretation that the uplands geology is likely deeply weathered siltstone and sandstone of the Lincoln Creek Formation, we used 10 feet as the upland soil depth, which includes both soil and likely portions of the deeply weathered bedrock throughout much of the uplands in the report area. The lowland dune sands do not have a bedrock failure plane, so we chose a failure plane depth based on the type of shallow landslides we would expect to observe on dunes, primarily flows, and selected 6 feet as the depth of the failure plane.

Dune sand is generally cohesionless; however, the older dunes inland from the beach are heavily vegetated and the fibrous roots of various plants have created an organic cohesion between the sand grains. Buchanan and Savigny (1990) attempted to quantify root cohesion in Whatcom County, in an area with vegetation similar to Ocean Shores and Westport peninsulas. Three sites assessed by Buchanan and Savigny (1990) contained sandy soils, so we used an average of the three sites and selected a cohesion value of 42 pounds/square foot for dune sand.

[2] "Soil" in this report is following engineering terminology that defines a soil as any unconsolidated sediment that is not bedrock.

Groundwater

The groundwater in beach and dune sand in the lowlands is very different from groundwater in the bedrock-derived upland soils. In the uplands, the silty clay loam soils retain water much longer and drain more slowly than well-drained dune sand. To better represent different ground water scenarios, we analyzed two soil saturation conditions: (1) during an intense or prolonged precipitation event and (2) dry season conditions, such as summer and early autumn. For depth to groundwater during a period of intense or prolonged precipitation, we selected 3 feet for dune sand and 0 feet (completely saturated) for upland soils. For depth to groundwater during drier conditions for dune sand, we selected unsaturated (no groundwater present) and for upland soils, 3 feet. Modeling high groundwater during an intense or prolonged precipitation event is a conservative approach and the worst-case scenario for landslide modeling. For all groundwater scenarios, the groundwater depth was assumed to be uniform throughout the study area for the soil type analyzed.

Shallow Landslides

Regional evaluation of shallow landslide vulnerability is best performed in a GIS. Spatial output is the a_c as grid data, which is easily combined with other spatial datasets in a GIS. We used the GIS program ESRI ArcGIS 10 to input rasterized topographic and soil properties data for the report area, similar to Jibson and others (1998, 2000). The ESRI application ModelBuilder was used to input equations to evaluate grid data.

Part of the a_c is the static factor of safety (FS_S), which describes the stability of a slope under normal (static) conditions and is calculated from the ratio of the forces resisting slope movement to the forces driving slope movement. The FS_S describes the stability of a slope under normal conditions, so a FS_S less than 1.0 indicates instability and a FS_S greater than 1.0 indicates stability. The greater the FS_S above 1.0, the more stable the slope; however, standard engineering practices generally require a FS_S greater than 1.3 to characterize an object as stable (U.S. Army Corps of Engineers, 2003).

To determine the FS_S for a regional analysis, a simplified model is used:

$$FS_s = \frac{c\prime}{\gamma t \sin\alpha} + \frac{\tan\varphi}{\tan\alpha} - \frac{m\gamma_w \tan\varphi}{\gamma \tan\alpha} \qquad \text{Equation 1}$$

where c' is the cohesion of the soil, φ is a soil's angle of internal friction, t is the slope-normal thickness of the potential failure slab, m is the proportion of the soil (slab) thickness that is saturated, α is the slope angle in degrees, γ is the soil unit weight, and γ_w is the unit weight of water (Harp and others, 2006; Jibson and others, 1998). When calculating m of the potential failure slab for soils over bedrock, we modeled groundwater at the surface (0 feet) and groundwater 3 feet below the surface, which were entered into Equation 1 as 1.0 and 0.7, respectively. For dune sand, we modeled groundwater at 3 feet below the surface and no groundwater, entered into Equation 1 as 0.5 and 0, respectively. In some grids on steep slopes where the FS_S was less than 1.0, indicating an actively failing slope, we forced those grids to 1.0 to represent the lowest possible FS_S.

The critical acceleration (a_c) is a function of the FS_S of a block and the gradient of a slope (Newmark, 1965) shown by:

$$a_c = (FS_S - 1)g \sin\alpha \qquad \text{Equation 2}$$

where FS_S is the static factor of safety, g is the acceleration due to gravity, and α is the angle of the slope in degrees. The spatial analyses evaluate the FS_S and a_c for each grid individually, so the properties of a grid are independent of the surrounding grids. In addition, despite unique model outputs for values in discrete grids, much of the input data is generalized for the report area, and output data is therefore not representative of site-specific conditions. Typical values used for soil properties of soil overlying bedrock in this analysis were 121 pounds/cubic foot for unit weight, 29 degrees for angle of internal friction, and 355 pounds/square foot for cohesion; for dune sand, 108 pounds/cubic foot for unit weight, 35 degrees for angle of internal friction, and 42 pounds/square foot for cohesion from roots. Material values of soils are from the Washington State Department of Transportation (2012 and unpub. documents, 2000, 1998, 1997, 1995), and root cohesion is from Buchanan and Savigny (1990).

DISCUSSION AND RESULTS

Shallow Rapid Landslides

The a_c should be considered a relative predictor of slope performance that indicates which slopes are more likely to fail under a given earthquake acceleration. The intent of the a_c output is to evaluate seismically induced slope instability and relative vulnerability to failure. Using a_c to identify areas above planned or existing tsunami evacuation routes with an increased risk of shallow landslide initiation is within the limited scope of this report. The relative nature of this model permits hazard assessment on a coarse (small) scale and may be used for community evacuation and hazard preparedness in conjunction with local and regional evaluation for earthquake emergency response. Because a_c was processed using a GIS, with very limited field verification and no site-specific laboratory tests of soil properties, evacuation routes that pass under areas of increased likelihood of seismically induced shallow landslides should be evaluated by an engineering geologist or geotechnical engineer. Sheets 1 and 2 illustrate the a_c from ground motions that the region might experience during a CSZ M9+ earthquake. The hazard ratings in Sheets 1 and 2 are qualitative indicators based on the difference between the a_c and PGA for each grid. High hazard is an a_c less than 0.2, medium hazard is an a_c between 0.2 and 0.3, and low hazard is an a_c between 0.3 and 0.4; slopes greater than 0.4 were not rated.

A principal hazard of shallow landslide initiation during an earthquake is debris blocking evacuation routes. The volume of sediment and debris necessary to halt passage of a passenger car is minimal, especially if trees are included in the debris. A CSZ tsunami would likely not permit evacuees the time to clear debris, so any seismically induced landslide that could potentially block a vehicle-dependent evacuation route must be evaluated. Routes that pass under a high hazard area require a detailed geotechnical investigation. An alternative to a geotechnical report would be rerouting the planned or existing evacuation route to reduce the risk of landslide-blocking.

In the lowlands, the primary areas of shallow landslide concern are the slopes of dunes stabilized by vegetation. The roots of plants increase cohesion by binding grains together, which permits slope gradient to increase beyond the angle of repose. Vegetated dunes that exceed an elevation of approximately 40 feet typically contain numerous slopes vulnerable to shallow landslides. At the time of analysis, approximately 5000 feet of the primary evacuation route for Ocean Shores on SR 115 passed under dune slopes vulnerable to shallow landslides. On the Westport peninsula the evacuation route on SR 105 passes under about 500 feet of slopes vulnerable to shallow landslides; however, the evacuation route is likely a sufficient distance from the slope, which significantly reduces the likelihood of debris blocking the route.

In the uplands, many of the slopes are vulnerable to seismically triggered shallow landslide initiation (Sheets 1 and 2). Steep slopes and deep soils contribute to this. Fortunately, no evacuation routes in the study area pass under slopes in the uplands, so landslide hazards in the uplands will not be discussed further in this report.

NEWMARK'S ANALYSIS

When assessing seismically induced shallow landslides, Jibson and others (1998), Capolongo and Refice (2002), and Jibson (2007) include Newmark's sliding block analysis as a means to estimate seismically induced slope performance. Newmark (1965) developed a method that models a landslide as a rigid block on an inclined plane and whose outputs are a prediction of the amount of movement on a slope during an earthquake. The method does not precisely predict the behavior of a slope, due to its simplified rigid-body displacement model, but it does provide a useful indicator of how a slope might perform during an earthquake (Jibson and others, 1998). Newmark's method is applicable at magnitudes between 5.5 and 7.6 (Jibson, 2007), significantly below the CSZ M9+ earthquake analyzed in this report. The methodology to calculate the Newmark displacement is based on empirical studies, and the modeled displacements must be compared to previous seismically induced landslides. Displacements are estimated for the total time ground motions exceed a_c. However, there hasn't been an instrumented M9+ event in the Pacific Northwest that can provide an empirical time-history for comparison purposes, nor is there an available synthetic time-history. Schulz and others (2012) modeled Newmark displacements using a time-history from the 2011 Tohoku-oki earthquake, but that subduction zone is significantly different from Cascadia so we do not regard this as typical. The predicted displacements must be used, instead, as a measure of the relative safety of slopes during and after a Cascadia event. There are other methods to calculate Newmark's method, such as modeling Arias intensity and using recorded peak ground acceleration from the Tohoku M9.0 earthquake in Japan (Schulz and others, 2012), but we feel that this is outside the project scope and an unnecessarily complicated step that adds an additional layer of assumptions.

Deep-Seated Landslides

Previous deep-seated landslide analyses in Aberdeen, Cosmopolis, and Hoquiam (Slaughter and others, 2013a) in geology similar to the uplands in the Westport Peninsula uplands found the results over-predict the hazard of seismically induced deep-seated landslide initiation. This was likely due to the modeling not taking into account various rock properties that influence slope stability. Detailed rock information requires a site-specific analysis, typically including drilling rock cores and laboratory testing of samples, data not available for the study area. Due to the lack of available subsurface data, Slaughter and others (2013a) used only one set of values for all deep-seated landslide analyses. There is a similar lack of detailed rock properties data for the study area, so no deep-seated landslide analyses were conducted in the uplands.

Appendix B. Technical Description of Liquefaction Susceptibility and Initiation Modeling from a Cascadia Subduction Zone M9+ Earthquake

INTRODUCTION

Seismically induced liquefaction can occur when saturated, cohesionless, granular soils[3] are subject to cyclic shear stresses, such as those generated by an earthquake. If pore water cannot escape the void spaces of a soil, the cyclic shear stresses increase hydrostatic pore pressure. If the hydrostatic pore pressure equals the overburden pressure of the soil, the effective stress of the soil becomes zero and the soil loses all strength and liquefies. The effects of liquefaction include sand blows, lateral spreading, loss of bearing strength, and structural settlement (Seed and Idriss, 1982). Soils identified as susceptible to liquefaction are generally sands and silty sands; however, there is recognition that, under certain conditions, fine-grained sediments have experienced seismically induced liquefaction (Seed and others, 2003; Bray and Sancio, 2006), and silt liquefaction was observed in a M5 earthquake in Puget Sound in 1995 (Walsh and Palmer, 1996; Palmer and Moses, 1996).

Historic records present valuable information for assessing the earthquake-induced soil liquefaction potential of an area. Chleborad and Schuster (1998) examined newspaper accounts of ground failures associated with two Puget Sound earthquakes—a M7.1 in the Olympia–Tacoma area on April 13, 1949, and a M6.5 in the Seattle area on April 29, 1965. Both earthquakes produced soil liquefaction that resulted in substantial damage to buildings, bridges, highways, railroads, water distribution systems, and marine faculties. During the 1949 event, liquefaction may have occurred on the geologically similar Long Beach peninsula, approximately 15 miles south of Westport. A front page article in the *Ilwaco Tribune* (1949) stated that "clam diggers report the earthquake was a blessing, as the clams, which have seemed scarce, came to the surface…."

Severe and prolonged ground shaking from a Cascadia subduction zone (CSZ) M9+ earthquake could persist for up to several minutes (Art Frankel, U.S. Geological Survey, written commun., 2008). The magnitude and duration of shaking could initiate severe damage throughout the Pacific Northwest, especially to infrastructure damaged by soils susceptible to liquefaction (Fig. 2). On the Washington coast, this damage may prevent efficient evacuation from an impending tsunami and impede post-tsunami rescue efforts. Although tsunami inundation zones have been modeled and evacuation routes planned (Walsh and others, 2000; WADGER, 2007a,b, 2012), there have been no detailed evaluations of soil initiation of liquefaction for evacuation routes in coastal communities. This appendix describes the technical background associated with soil liquefaction susceptibility and initiation analysis for the Ocean Shores and Westport peninsulas in Grays Harbor County, Washington. The outputs of this analysis are intended for preliminary screening of areas vulnerable to seismically induced liquefaction.

The intent of the map is as a regional planning tool and not for site-specific analysis. This map cannot be used to determine the presence or absence of liquefiable soils in any specific locality. This map cannot be substituted for a site-specific geotechnical investigation, which must be performed by qualified practitioners and is required to assess the potential for ground failures and consequent damage at a given locality. Likewise, we present no estimate of the damage resulting from liquefaction; in some instances, liquefaction may occur without causing significant ground displacement and consequent damages to structures.

BACKGROUND

Previous liquefaction susceptibility studies in Washington State include evaluation of the Seattle area (Grant and others, 1998), portions of the greater Puget Sound (for example: Palmer and others, 2003, 2002, 1994), and reconnaissance maps for all Washington counties (Palmer and others, 2004). The only maps that cover the area of interest are the maps of Washington counties; however, these maps are based on 1:100,000-scale geology and published correlations of geologic units susceptible to liquefaction and do not include soil thickness information (Palmer and others, 2004). Other published liquefaction studies include a manual and computer program with

[3] "Soil" in this report is following the engineering terminology that defines a soil as any unconsolidated sediment that is not bedrock.

guidance for evaluating liquefaction hazards in Washington State developed by Kramer (2008) for the Washington State Department of Transportation (WSDOT).

METHODS

This report includes a hazard map delineating zones vulnerable to initiation of liquefaction. Construction of the hazard map required several datasets, including geotechnical borehole logs, soils mapping, geologic mapping, a lidar (light detection and ranging) digital elevation model (DEM), and aerial imagery. The following section describes the datasets and details the steps necessary to construct the hazard map.

Geotechnical Borehole Logs

Boring logs typically contain data on subsurface soil properties and are required in many communities before beginning any significant public works or construction project. A total of three reports documenting 29 geotechnical borings (Sheet 3) in the study area were obtained from the Washington State Department of Transportation (WSDOT), private companies, and other government agencies. For this analysis, we wanted to use borings that exceeded a depth of 40 feet, contained soil penetration test (SPT) N-values[4] in a minimum of 5-foot increments, and included descriptions of discrete soil layers. When a site contained several borehole logs in a small area (typically a city block), we omitted all but the deepest log with the greatest SPT values per foot. Of the 29 borings, only four[5] exceeded 40 feet (all WSDOT boreholes), so we used borehole logs as shallow as 10 feet deep for liquefaction analysis.

Boring logs typically contain empirical soil descriptions or soils categorized by the Unified Soil Classification System (USCS), SPT N-values, layer thickness, and depth to groundwater at time of drilling. Some logs also contain lab data detailing soil properties, such as soil moisture content, dry unit weight, Atterberg limits, and sediment size. These data were input into the program WSliq, which can analyze the liquefaction susceptibility, initiation, and effects at a borehole (Kramer, 2008). The majority of borehole logs did not contain analytical soil properties, so we averaged existing analytical soil properties data to create one input value for each USCS soil in the report area (Table B1). The averaged values include the plasticity index, unit weight, and fines content. This likely underestimated the liquefaction hazard of some boreholes, but due to a lack of analytical lab data and homogeneous sedimentology of the area, we felt the technique was justified to simplify the datasets.

Table B1. USCS soil properties for boreholes analyzed for the report area.

USCS symbol	Dry unit weight[3] (pcf)	Plasticity index[1]	Fines[2,4] (%)	Description
GM	128	4	25	silty gravels, poorly graded gravel-sand-silt
SP	110	0	5*	poorly graded clean sands, sand-gravel mix
SM	111	5	25*	silty sands, poorly graded sand-silt mix; sandy loam
SM-SC	120	9	25	sand-silt clay mix with slightly plastic fines
ML	107	11	60	inorganic silts and clayey silts; silt loam

[1] Transportation Research Board, 2001, Appendix CC
[2] WSDOT, 2012
[3] Koloski and others, 1989
[4] U.S. Bureau of Reclamation, 1998
* Palmer and others, 2002

[4] SPT (standard penetration test) N-value is the result of a data collection technique for subsurface soils. The SPT is performed during the advancement of a soil boring to obtain an approximate measure of the dynamic soil resistance, as well as a disturbed soil sample (Mayne and others, 2001). SPTs are standard practice for most geotechnical boring projects and can be found in borehole logs for most geotechnical reports. The SPT consists of a 140-pound hammer dropped 30 inches onto a split-spoon sampler at the bottom of a borehole and the blows (N-values) necessary to drive a split-spoon sampler 12 inches are recorded. SPTs can also be taken using different size samplers or with an automatic trip hammer. In granular soils, an SPT is typically conducted at regular depth intervals, and in cohesive soils, an SPT may be conducted at each stratum encountered during boring (Mayne and others, 2001). N-values can be correlated to the apparent density and consistency of the soil and used in conjunction with observed and measured soil properties to estimate liquefaction susceptibility. Assuming that a sample is collected in the split-spoon sampler, a disturbed soil sample can be analyzed in a lab for material properties and USCS soil classification.

[5] The four WSDOT boreholes were for a bridge project. Two boreholes were drilled 150 feet apart, and soils were sampled to a depth of approximately 75 feet. Six months later, WSDOT returned to the same location and drilled boreholes adjacent to the previous boreholes, this time sampling from approximately 75 feet to depths exceeding 115 feet. Because we are interested in only the upper 40 feet of a borehole, we analyzed the shallower two of the four boreholes.

The depth to groundwater is an important input in WSliq, and we used two scenarios to represent seasonal variations: groundwater at the surface (0 feet) and groundwater 3 feet below the surface. Both scenarios represent groundwater levels during months with a high water table. Groundwater at the surface is intended to reflect conditions associated with prolonged and intense precipitation when the ground is completely saturated. Though full saturation is likely not realistic, it represents a conservative mapping approach and the worst-case scenario for groundwater conditions and is a necessary assumption to simplify model inputs. For both groundwater scenarios, the groundwater depth was assumed to be uniform throughout the region.

In areas of artificial fill, we assumed that the entire fill was vulnerable to liquefaction initiation, even if WSliq indicated that it was not. This is because the fill was likely applied without any engineering, so soil properties are highly variable throughout the spatial extent of the fill. We used historic mapping and soil mapping to delineate the extent of artificial fill in the report area (Sheet 3).

Groundwater and Wetlands

Neither peninsula appears to have a groundwater monitoring program that permits accurate calculation of the depth to groundwater in the unconsolidated sands. Due to the numerous geologic and geomorphic similarities of the study area to the Long Beach peninsula, we used a U.S. Geological Survey (USGS) project on the Long Beach peninsula as an analog for groundwater conditions on the Westport and Ocean Shores peninsulas. On the Long Beach peninsula, the USGS installed 120 groundwater monitoring wells and monitored monthly groundwater levels for 1 to 1.5 years, depending on the site (Thomas, 1995). Slaughter and others (2013b) examined groundwater levels during the wettest and driest months, January and October, respectively. It was shown that groundwater elevation does not mimic the topography as is typically observed and, instead, groundwater elevation remains relatively flat at or below an elevation of 15 feet across much of the peninsula. Groundwater was not present in the prominent dunes, likely due to the well-drained, permeable dune sands that transmit water quickly to the underlying water table and drainage channels constructed to lower the groundwater table. In low elevation areas on the Long Beach Peninsula, groundwater is very shallow, hence the abundance of wetlands that is also observed on the Ocean Shores and Westport peninsulas. A GIS analysis of a spatial wetland inventory to a lidar DEM shows that the average elevation of all wetlands on the Long Beach, Ocean Shores, and Westport peninsulas is approximately 14 feet. The average surface elevation of the three peninsulas, not including the uplands, is 17 feet. Based on these similar geomorphic and groundwater features, we feel the comparison between the peninsulas is appropriate.

The wetlands inventory catalogued in the National Wetlands Inventory (U.S. Fish and Wildlife Service, 2012) is a reconnaissance dataset created using the analysis of high-altitude imagery to categorize wetlands based on vegetation, visible hydrology, and geography. The spatial database identifies more than 2268 acres of wetlands on the peninsulas. The dataset is based on a remote analysis that lacks field reconnaissance, so it contains an inherent unquantified margin of error; however, based on our own observations on the peninsula and our own analysis of infrared imagery and lidar data, we found the dataset to be accurate at the scale of mapping we present in this report.

Liquefaction Susceptibility and Initiation Analysis

The process of liquefaction hazard analysis is divided into three aspects: susceptibility, initiation, and effects (Kramer, 2008). Because of the large report area, we are analyzing only liquefaction susceptibility and initiation. Analysis of liquefaction effects is best suited to site-specific analysis and is outside of the scope of this project.

The first step in an analysis is to determine whether a soil is susceptible to liquefaction. A soil is considered susceptible to liquefaction if it can liquefy under some level of loading and a non-susceptible soil cannot liquefy—no matter how strong the loading (Kramer, 2008). Kramer outlines a simple analysis to estimate the relative liquefaction susceptibility at the deposit-level (that is, the uppermost soil layer). Preliminary screening of liquefaction susceptibility is based on the Susceptibility Rating Factor (SRF), which is defined as follows:

$$SRF = F_{hist} \, x \, F_{geology} \, x \, F_{comp} \, x \, F_{gw}$$

where F_{hist} is the liquefaction history factor, $F_{geology}$ is the geology factor, F_{comp} is the composition factor, and F_{gw} is the groundwater factor. Kramer describes detailed procedures to determine the values of the four factors. When the SRF is computed according to these procedures, the susceptibility to liquefaction of a site can be estimated from Table B2. The SRF is a generalized analysis of liquefaction susceptibility that requires only the most basic of inputs; however, the output can be easily transferred to a spatial dataset to represent areas susceptible to liquefaction.

A more detailed susceptibility analysis is part of the computer program WSliq (Kramer, 2008) that analyzes multiple soil layers in a geotechnical borehole. The program, developed for the Washington Department of Transportation (WSDOT), can evaluate liquefaction susceptibility, initiation, and effects for all soil layers in a borehole, given appropriate soil property data inputs. The results of the susceptibility evaluation are expressed in terms of susceptibility index (SI) values. The SI values can be weighted to follow the analysis procedures of Boulanger and Idriss (2005) or Bray and Sancio (2006) or any ratio of the two—we chose to weight them equally. The SI indicates whether a soil layer is susceptible to liquefaction; however, a soil may not liquefy if the anticipated level of ground shaking is not sufficient to overcome the inherent liquefaction resistance of the soil (Kramer, 2008), so initiation of liquefaction must then be calculated.

Table B2. Characterization of overall site susceptibility to liquefaction hazards.

SRF	Site susceptibility
0 – 5	very low
5 – 10	low
10 – 25	moderate
25 – 50	high
> 50	very high

Based on the same data as the susceptibility analysis, WSliq calculates the initiation of liquefaction factor of safety for each layer in a borehole. The program can analyze earthquake-induced initiation of liquefaction in a single scenario, multiple-scenarios, and a performance-based scenario. We selected the single-scenario analysis to evaluate liquefaction potential from a CSZ M9+. WSliq provides three methods to calculate the factor of safety, following techniques from Youd and others (2001), Boulanger and Idriss (2004), and Cetin and others (2004). The three procedures provide the best currently available coverage of initiation of liquefaction. Each has advantages and limitations, and none can be considered clearly superior to the others (Kramer, 2008). Because of this, we elected to average the factor of safety outputs from all three procedures. The averaged factor of safety for each stratum was evaluated for the upper 40 feet of the borehole, and we calculated the percentage of the borehole vulnerable to initiation of liquefaction following Palmer and others (2003, 2002, 1994). We then assigned a semiquantitative hazard rating based on the percentage of the upper 40 feet vulnerable to initiation of liquefaction (Table B3) and entered the hazard rating into a GIS. We considered a factor of safety less than 1.0 as vulnerable to initiation of liquefaction. Because peat is not liquefiable, we did not include peat in the hazard rating.

Table B3. Criteria used in this report to provide a soil liquefaction hazard rating (from Palmer and others, 2002).

Percent of borehole vulnerable to initiation of liquefaction	Borehole hazard rating
> 50	high
25 – 50	moderate
5 – 25	low
< 5	very low

Seismic Survey

Active and passive shallow seismic surveys were conducted to model the shallow seismic (shear-wave velocity) behavior at Ocosta Elementary School (Sheet 3) on the Westport peninsula: Multi-channel Analysis of Surface Waves (MASW) as an active survey and Microtremor Array Measurements (MAM) as a passive survey. Collected data were processed using SeisImager 2D/SW software. National Earthquake Hazards Reduction Program (NEHRP) recommended site classifications for calculated V_{s100} values were determined from shallow shear-wave velocity profiles obtained from surface-wave data processing for each site and calculated average shear-wave velocities for the upper 100 feet (V_{s100}). Shear-wave velocity (V_s) values for depths less than 100 feet are well determined using MASW/MAM methods. See Cakir and Walsh (2012) for details of the methodology.

Liquefaction Hazard Mapping

The interpretation of the hazard rating of initiation of liquefaction for individual boreholes into a spatial dataset representing zones of similar liquefaction potential requires integration of several datasets including geology and soil mapping (polygons), liquefaction susceptibility index spatial data, borehole liquefaction hazard rating point data, lidar interpretation, and wetlands spatial data. Geology and soil data were input into the SRF calculation to identify generalized zones susceptible to liquefaction. Lidar interpretation identified areas of localized fill applied for individual buildings, parking lots, and other public and private works. This is important to identify areas of fill that may not be engineered and are likely more vulnerable to initiation of liquefaction. Wetlands data identified areas of potential high groundwater table that could increase the likelihood of liquefaction initiation and susceptibility. These areas typically coincided with peat zones identified in the soils layer; however, peat was typically mapped as a much smaller area than the actual wetland.

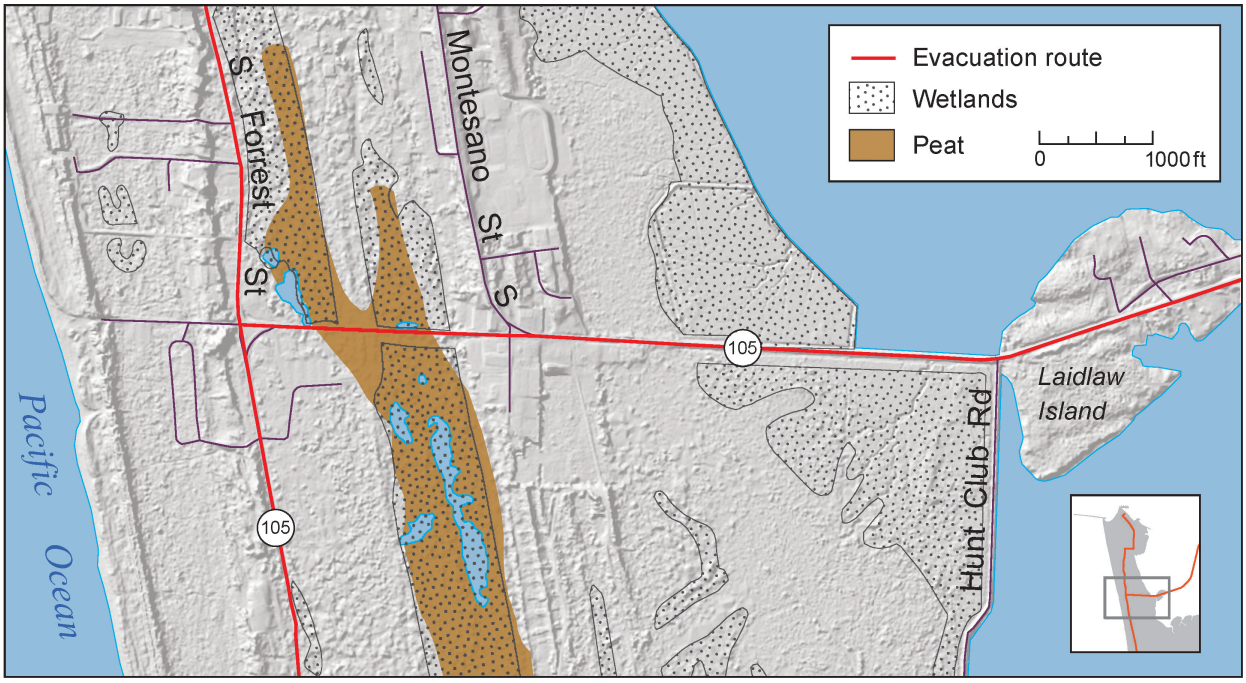

Figure B1. An evacuation route crossing peat deposits and wetlands on the Westport peninsula. Evacuation routes are red, brown polygon indicates peat, and stippling indicates wetlands.

DISCUSSION AND RESULTS

Analysis of the few boreholes in the report area indicates that the peninsula is susceptible to liquefaction from seismic loading produced by a CSZ M9+ event. However, despite the unconsolidated sediments consisting primarily of sand, sediment considered highly liquefiable, initiation of liquefaction of sand on the peninsula ranges from very low to low. The exceptions are Westhaven Cove marina in Westport and areas of likely artificial fill where liquefaction initiation and susceptibility are high. Mapping of soils and wetlands indicates that 46 percent of the peninsula contains peat and (or) wetlands. Peat is not liquefiable, but is still considered at risk for deformation and sand boils from underlying liquefiable sediments. Wetlands indicate a high groundwater table that could increase the liquefaction susceptibility and initiation of beach and dune sands that coincide with a wetland, due to the increased available of groundwater.

Liquefaction Susceptibility and Initiation

Liquefaction analysis provides both a calculation of the factor of safety for soil in individual boreholes (Appendix C) and the relative vulnerability of an area to initiation of liquefaction associated with ground shaking from a CSZ M9+ earthquake (Sheet 3). Unfortunately, the limited quantity of boreholes makes the extrapolation to spatial hazard mapping data difficult, so less-detailed datasets are used in the analysis. The primary datasets are the soils survey (Pringle, 1986) and lidar DEM. The lidar DEM allows for identification of high dunes that may be less vulnerable to initiation of liquefaction due to the absence of available groundwater. The soils survey identifies soil types based on parent material, such as “wind-blown sand”, “beach deposits”, “sandy alluvium”, or “peat or decomposed organic material”. Though sand must be considered susceptible to liquefaction, sand may not experience initiation of liquefaction if it is in a very dense state (Kramer, 2008), which the few boreholes on the Ocean Shores peninsula suggest. Borehole calculations indicate that areas in sand with low initiation of liquefaction are in the low-elevation areas of the peninsulas identified as wind-blown sand in the soils mapping. The soil mapping appears to contradict the borehole information and identifies all the boreholes in wind-blown sand, such as dune and interdune sand. Windblown sand is not compacted by waves so has an increased likelihood of initiation of liquefaction. This discrepancy between borehole and soil mapping data is likely because soil surveys investigate the upper 60 inches of a soil, whereas boreholes investigate typically well below 60 inches in the subsurface. Many of the boreholes in

Appendix C show an average factor of safety less than 1.0 for the first soil sample while deeper soil samples' factors of safety exceed 1.0, suggesting wind-blown sands overlaying wave-compacted beach sands.

Without detailed borehole data across both peninsulas, it is not possible to better define the initiation of liquefaction, so the analysis is based on descriptive terms of soils. Any low-elevation areas defined by the soil survey as "sandy alluvium", not "peat" or "wind-blown sand", are considered some form of beach deposits that have been compacted by waves. Peat and wind-blown sand (hereafter dune sand and interdune sand) are discussed below.

Parallel to the beaches are localized deposits of dune and interdune sand, both transported by wind. These features are not compacted by waves and therefore have an increased vulnerability to initiation of liquefaction. Sand dunes are small hills of well-drained sand that do not contain the necessary groundwater to initiate liquefaction. The lack of compaction and lack of groundwater on sand dunes categorizes them as low hazard for initiation of liquefaction. To reflect the reduced liquefaction hazard of sand dunes, we used lidar to delineate sand dunes exceeding 25 feet above mean sea level and lowered their liquefaction hazard to very low or low to reflect the lack of available groundwater.

The sands most vulnerable to initiation of liquefaction are interdune sands where shallow groundwater may be present. Wetlands cover 2268 acres (42%) of the peninsulas. Areas where they interface with interdune sand have an increased vulnerability to liquefaction due to the availability of water in the subsurface. These low-elevation areas are categorized as low to moderate hazard for liquefaction.

Peat covers nearly 987 acres of the peninsulas (Sheet 3), and though peat cannot liquefy, it may be subject to vertical compaction and consequent settlement caused by ground shaking. Also, sand layers interbedded with the peat deposits may be liquefiable (Palmer and others, 2002). These are significant concerns for roads and structures built on peat. Peat deposits on the peninsulas trend north–south and are crossed by some roads. One concern is that the roads may not have adequate engineering to prevent road failure due to seismically induced peat settlement, deformation, or compaction. Examples of roads crossing peat are SR 115 on the Ocean Shores peninsula and SR 105 on the Westport peninsula (Fig. B1), both tsunami evacuation routes. One road failure at any of the peat deposits could render a road potentially impassable to passenger car traffic. Furthermore, the mapped peat is likely the *minimum* distribution of peat on the peninsulas, and it is possible that peat covers a larger area of the surface and subsurface. Areas of unmapped peat may include wetlands and other low-elevation locations throughout the peninsulas.

Artificial fill is commonly vulnerable to initiation of liquefaction and the only identified site of significant fill is at Westhaven Cove at Westport. Detailed construction records are lacking for the cove, so we based our mapping on analysis of historic USGS mapping and a draft environmental assessment (U.S. Army Corps of Engineers, 2013) that describes a brief history of Westhaven Cove. According to the 2013 report, the U.S. Army Corps of Engineers enlarged Westhaven Cove in the 1950s, and it is likely that the waterfront area was filled in with dredge materials excavated to create the harbor, similar to other harbor projects in the state, such as Ilwaco in Pacific County. Dredge fills were typically applied without regard to engineering properties or application technique, creating soils potentially very vulnerable to initiation of liquefaction. The liquefaction hazard for the port is difficult to quantify because of the high variability of soil properties of fill and lack of subsurface data. However, historic evidence of fills that experienced seismic shaking, such as from the M6.5 1965 Seattle-area event, reported significant initiation of liquefaction of non-engineered fills. Thus we consider all documented or suspected non-engineered fill as highly vulnerable to initiation of liquefaction.

The liquefaction analyses provide both a relative vulnerability to initiation of liquefaction, in the form of hazard mapping, and a calculation of the factor of safety for individual boreholes associated with ground shaking from a CSZ M9+ earthquake (Appendix C). Based on similar research on the Long Beach peninsula, the liquefaction hazard mapping shows that all low-lying areas on the Ocean Shores and Westport peninsulas are underlain by sediments susceptible to liquefaction or deformation. The interaction of low-lying sands with mapped wetlands may increase the liquefaction hazards due to the availability of water. The only area recognized as high hazard is the suspected dredged fill used to create Westhaven Cove in Westport. Peat deposits on both peninsulas are vulnerable to deformation, sand boils, and compression; however, there is no way to quantify the hazard other than acknowledging the concern—mitigating for peat should be considered when building roads. The hazard map is a preliminary product that requires considerable refinement with the addition of subsurface geotechnical data.

Seismic Survey to Determine Shear-wave Velocity

Site class is a simplified method for characterizing the ground-motion amplifying effects of soft soils during an earthquake by evaluating the relation of average shear-wave velocity in the upper 100 feet of the soil–rock column to the amplification of shaking at ground surface (Palmer and others, 2004). The site classes are based on the National Earthquake Hazard Reduction Program (NEHRP) seismic site classification. Shear-wave velocity results at the Ocosta Elementary School on the Westport peninsula show a low average shear-wave velocity (V_{s100}). For comparison, we included four sites from the Long Beach peninsula (see Slaughter and others, 2013b, for an explanation and location of the survey sites), specifically, Pacific Pines State Park, Ocean Park Elementary, Loomis Lake State Park, and Washington State University Extension. All Long Beach and Westport peninsula sites are classified as site class D, which represents softer soil conditions that result in the amplification of ground shaking (Fig. B2) and is interpreted as having a moderate to high vulnerability to liquefaction. This supports the geologic and liquefaction mapping at the elementary school and across the Westport peninsula; however, it does not recognize the potential lack of groundwater on the dunes, which significantly decreases the liquefaction hazard. This survey also does not capture the difference between dune and beach sands. The Long Beach peninsula sites are all located in beach sands and the upper approximately 25 feet of the Westport peninsula site is located on dune sand likely overlying beach sand.

Shear-wave velocity for liquefaction analysis has several disadvantages compared to the soil penetration test (SPT). Idriss and Boulanger (2008) state that shear-wave velocity provides very limited spatial resolution for characterizing site stratigraphy and heterogeneity and is not a sensitive measure of liquefaction resistance, but can be useful where no other data are available. The seismic survey reveals a similar NEHRP site class for all sites as well as a generally similar graph (Fig. B2) suggesting analogous sediment properties.

Table B4. National Earthquake Hazards Reduction Program (NEHRP) recommended site classifications.

Site name	Location	NEHRP site class
Ocosta Elementary School	Westport peninsula	D
Pacific Pines State Park	Long Beach peninsula	D
Ocean Park Elementary	Long Beach peninsula	D
Loomis Lake State Park	Long Beach peninsula	D
Washington State University Extension	Long Beach peninsula	D

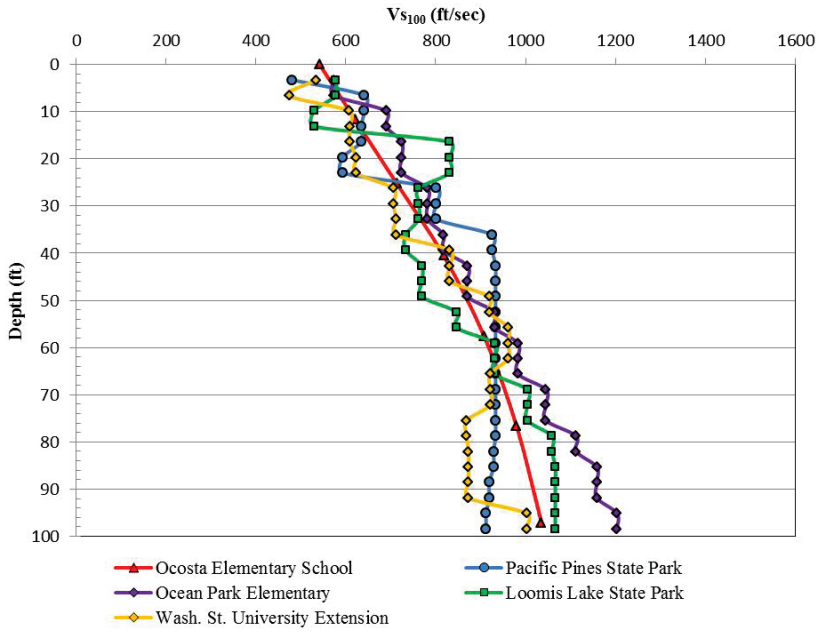

Figure B2. Active and passive shallow seismic survey V_{s100} data at Ocosta Elementary School on the Westport peninsula and four additional locations from the Long Beach peninsula (see Slaughter and others, 2013b, for explanation and location of Long Beach peninsula data). See Table B4 for the peninsula on which each site is located.

Appendix C. Analyzed Borehole Data Table

Boreholes analyzed in WSliq (Kramer, 2008) produced output tables defining the calculated liquefaction susceptibility and initiation values for each layer in a borehole. See Kramer (2008) for a detailed description of the process. The following are descriptions of the column headings for the tables below:

- **Layer:** The sequential number of the stratigraphic layer subdivided by the N-value. For input into WSliq each N-value was treated as an individual layer within a sedimentary unit, so layers do not match the stratigraphy of the borehole. For instance, if a layer of continuous silt was 23 feet thick and had four N-values, we would divide the silt layer into four layers 4.75 feet thick, each with its own N-value.
- **USCS:** Unified Soil Classification System two-letter description of a soil unit. See Table B1 for definitions.
- **z:** Thickness of the layer in feet.
- **Nm:** SPT (standard penetration test) N-value blow count necessary to drive a split-spoon sampler 12 inches into the bottom of a borehole.
- **B-I:** Liquefaction susceptibility index based on Boulanger and Idriss (2005).
- **B-S:** Liquefaction susceptibility index based on Bray and Sancio (2006).
- **SI:** Liquefaction susceptibility index based on the average of the B-I and B-S values.
- **Liq potential:** Liquefaction potential of the layer based on the SI.
- **NCEER:** National Center for Earthquake Engineering Research; factor of safety calculation.
- **B&I:** Boulanger and Idriss (2004); factor of safety calculation.
- **Cetin:** Cetin and others (2004); factor of safety calculation.

Table C1. Initiation of liquefaction in terms of the factor of safety (FS) for a layer, based on three methods available in WSliq. The procedures provide the best currently available coverage of initiation of liquefaction and each has advantages and limitations with respect to the others and none can be considered to be clearly superior to the others. Because of this, we elected to average the factor of safety outputs from all three procedures for each layer in a borehole. Only layers that are susceptible to liquefaction have their initiation of liquefaction calculated. Note that a layer may be susceptible to liquefaction, but the FS may not fall below 1.0, indicating the layer is modeled not to initiate liquefaction. Also, layers identified as fill were assumed to fail during a M9+ CSZ earthquake, regardless of the FS values calculated in WSliq. NCEER, National Center for Earthquake Engineering Research from Youd and others (2001); B&I, Boulanger and Idriss (2004); Cetin: Cetin and others (2004).

CONVENTION CENTER B-1

Layer	USCS	z (ft)	Nm	B-I	B-S	SI	Liq potential	NCEER	B&I	Cetin
1	SM	5	7	0.62	0.45	0.54	YES	0.20	0.19	0.30
2	SM	3	22	0.62	0.45	0.54	YES	3.25	3.37	1.70
3	SM	2	56	0.62	0.45	0.54	YES	3.29	3.37	5.06
4	SM	1	70	0.62	0.45	0.54	YES	3.31	3.36	5.06
5	SM	4	49	0.62	0.45	0.54	YES	3.34	3.36	5.06
6	SM	6	29	0.62	0.45	0.54	YES	3.42	3.36	3.22
7	SM	6	43	0.62	0.45	0.54	YES	3.54	3.36	5.08

LOOP ROAD B-1

Layer	USCS	z (ft)	Nm	B-I	B-S	SI	Liq potential	NCEER	B&I	Cetin
1	SM	3	32	0.62	0.45	0.54	YES	3.19	3.37	5.05
2	SM	2	15	0.62	0.45	0.54	YES	3.22	0.59	0.77
3	SM	3	21	0.62	0.45	0.54	YES	3.26	3.37	1.47
4	SM	4	31	0.62	0.45	0.54	YES	3.31	3.36	4.86

LOOP ROAD B-4

Layer	USCS	z (ft)	Nm	B-I	B-S	SI	Liq potential	NCEER	B&I	Cetin
1	SM	4	16	0.62	0.45	0.54	YES	3.20	0.76	1.03
2	SM	4	15	0.62	0.45	0.54	YES	3.25	0.59	0.68
3	SM	4	14	0.62	0.45	0.54	YES	3.30	0.47	0.52

LOOP ROAD B-6

Layer	USCS	z (ft)	Nm	B-I	B-S	SI	Liq potential	NCEER	B&I	Cetin
1	SM	4	11	0.62	0.45	0.54	YES	0.31	0.30	0.53
2	SM	5	19	0.62	0.45	0.54	YES	3.26	2.16	1.12
3	SM	6	55	0.62	0.45	0.54	YES	3.34	3.36	5.06
4	SM	2	70	0.62	0.45	0.54	YES	3.41	3.36	5.06

LOOP ROAD B-7

Layer	USCS	z (ft)	Nm	B-I	B-S	SI	Liq potential	NCEER	B&I	Cetin
1	SM	3	6	0.62	0.45	0.54	YES	0.18	0.18	0.30
2	SM	2.5	16	0.62	0.45	0.54	YES	3.23	0.76	0.84
3	SM	5.5	40	0.62	0.45	0.54	YES	3.29	3.37	5.07

LOOP ROAD B-9

Layer	USCS	z (ft)	Nm	B-I	B-S	SI	Liq potential	NCEER	B&I	Cetin
1	SM	3	12	0.62	0.45	0.54	YES	0.36	0.34	0.66
2	SM	3	10	0.62	0.45	0.54	YES	0.28	0.26	0.38

LOOP ROAD B-13

Layer	USCS	z (ft)	Nm	B-I	B-S	SI	Liq potential	NCEER	B&I	Cetin
1	SM	4	14	0.62	0.45	0.54	YES	3.20	0.47	0.79
2	SM	2	24	0.62	0.45	0.54	YES	3.24	3.37	2.30

WSDOT 17 TH-1-03

Layer	USCS	z (ft)	Nm	B-I	B-S	SI	Liq potential	NCEER	B&I	Cetin
1	SP	7	2	1	0.45	0.73	YES	0.06	0.08	0.12
2	SP	5	19	1	0.45	0.73	YES	2.97	1.60	1.04
3	SP-SM	5	19	1	0.45	0.73	YES	3.06	1.39	1.08
4	SP-SM	5	22	1	0.45	0.73	YES	3.19	1.65	1.19
5	SP-SM	5	20	1	0.45	0.73	YES	3.31	0.65	0.65
6	SP-SM	5	22	1	0.45	0.73	YES	3.46	0.72	0.63
7	SP-SM	5	30	1	0.45	0.73	YES	3.65	3.10	1.19
8	SP-SM	5	25	1	0.45	0.73	YES	3.85	0.83	0.61

WSDOT 17 TH-2-03

Layer	USCS	z (ft)	Nm	B-I	B-S	SI	Liq potential	NCEER	B&I	Cetin
1	SP	5	4	1	0.45	0.73	YES	0.09	0.11	0.18
2	SP	5	15	1	0.45	0.73	YES	0.33	0.34	0.51
3	SP	5	19	1	0.45	0.73	YES	3.31	0.57	0.72
4	SP	5	21	1	0.45	0.73	YES	3.39	0.53	0.85
5	SP	5	25	1	0.45	0.73	YES	3.50	0.71	0.93
6	SP	5	18	1	0.45	0.73	YES	0.31	0.26	0.35
7	SP	8	6	1	0.45	0.73	YES	0.11	0.11	0.10
8	SP	3	45	1	0.45	0.73	YES	4.08	3.33	2.40